

BEM coupling with the FEM fictitious domain approach for the solution of the exterior Poisson problem and of wave scattering by rotating rigid bodies

Original

BEM coupling with the FEM fictitious domain approach for the solution of the exterior Poisson problem and of wave scattering by rotating rigid bodies / Falletta, Silvia. - In: IMA JOURNAL OF NUMERICAL ANALYSIS. - ISSN 1464-3642. - STAMPA. - 38:2(2018), pp. 779-809. [10.1093/imanum/drw073]

Availability:

This version is available at: 11583/2671114 since: 2019-09-04T13:09:32Z

Publisher:

Oxford University Press

Published

DOI:10.1093/imanum/drw073

Terms of use:

This article is made available under terms and conditions as specified in the corresponding bibliographic description in the repository

Publisher copyright

Oxford University Press postprint/Author's Accepted Manuscript

(Article begins on next page)

BEM coupling with the FEM-fictitious domain approach for the solution of the exterior Poisson problem and of the wave scattering by rotating rigid bodies *

S. Falletta[†]

Abstract

We consider two exterior model problems in 2D: the Poisson equation and the problem of waves scattered by rotating rigid bodies. The exterior domain is the \mathbb{R}^2 complement of a bounded rigid obstacle, subject to a rotation in the time dependent case. By using a fictitious domain approach, we artificially extend the solution in the whole \mathbb{R}^2 . Then, we propose and study a Finite Element-Boundary Element (FEM-BEM) coupling method for the solution of the problem in a finite computational domain, delimited by an artificial boundary \mathcal{B} . The transmission conditions between the interior and exterior domain are imposed on \mathcal{B} by a boundary integral equation coupled first to the Poisson, and then to the wave equation, these being defined in the interior domain. The Dirichlet conditions on the boundary of the physical obstacle are enforced weakly, by means of Lagrange multipliers. The main advantage of this approach is that the finite element mesh can be chosen independently of the geometry of the obstacle. Moreover, in the time dependent case, the proposed method allows to use a given fixed mesh, thus avoiding the complexity of constructing at each time step a new finite element computational mesh.

For the Poisson problem we obtain convergence results when the space discretization is performed by standard finite elements in the interior domain and by a Galerkin boundary element method on \mathcal{B} . For the wave equation, we perform a full space discretization by finite elements, coupled with a Crank-Nicolson time-stepping scheme. On the boundary \mathcal{B} , a boundary element method and a convolution quadrature based on a BDF method of order 2 are used. We present numerical results for non trivial data, which validate the proposed numerical approach. In the wave equation case, these include also rotating obstacles and external sources.

keywords: wave equation; boundary element method; finite element method; fictitious domain; numerical methods.

*This work was supported by the Ministero dell'Istruzione, dell'Università e della Ricerca of Italy, under the research program PRIN 2012: Innovative methodologies for PDE-based numerical modelling, and by the GNCS-INDAM 2015 research program: Isogeometric analysis and boundary element methods.

[†]Dipartimento di Scienze Matematiche, Politecnico di Torino, Italy. Email: silvia.falletta@polito.it

1 Introduction

Boundary element methods provide a very appealing way to deal with problems in unbounded exterior domains. They are based on integral operators defined on the boundary of the physical domain, and they offer the great advantage of describing the solution only by its boundary values, thus reducing the problem dimensions by one. Hence, only a discretization of the boundary is necessary, which significantly reduces the number of unknowns, if compared, for example, to domain discretization methods such as finite elements. Once the density function is retrieved (by solving the corresponding boundary integral equation), the solution of the original problem at any point of the exterior domain is obtained by computing boundary integrals. This procedure may however result not efficient, especially when the solution is needed at many points of the infinite domain.

Alternatively, and when, for example, the material of the exterior domain presents varying characteristics, domain discretization methods such as finite elements can be used. In this case, having defined the bounded computational domain, where one is interested in studying the behavior of the solution, a key issue is the introduction of proper (transparent) boundary conditions. These must guarantee that the solution of the initial-boundary value problem inside the finite computational domain coincides with the restriction of the solution of the original problem. This leads to FEM-BEM like coupling strategies. The finite element method is used as a solver in the finite computational domain; the boundary element method is used as a Non Reflecting Boundary Condition (NRBC), which defines a relationship between the solution of the differential problem and its normal derivative on the chosen artificial boundary that delimits the computational domain.

The finite element method relies on geometry-fitted meshes, meaning that the union of the mesh cells closely approximates the domain on which the problem is defined. When the geometry of the domain is complicated, meshes of small size have to be considered in order to follow exactly the shape of the object. This can be a drawback from the implementation point of view, because the efficiency of the computation is decreased by the unstructured nature of the data. As an alternative approach, one can consider the fictitious domain method (even known as “domain embedding” method). The fictitious domain method consists in immersing the original physical domain in a geometrically larger and simply-shaped one (called fictitious domain) and in imposing the boundary conditions on the boundary of the physical domain in a weak form, by means of Lagrange multipliers. The advantage of this approach is that the problem is solved in a simpler enlarged domain that contains the scatterer; the differential and the boundary operators are to some extent separated, so that the finite element mesh can be chosen independently of the geometry of the obstacle. The boundary conditions on the scatterer are taken care of by an operator acting on a lower dimensional space.

The fictitious domain method has been introduced in [21] and successfully applied to stationary problems with complex geometries ([25]) and to time dependent problems such as acoustic wave propagation problems ([38]), electromagnetic scattering ([13]) or elastic wave propagation ([7]). In all the mentioned papers stationary obstacles have been considered and local absorbing boundary conditions or PML methods have been used for the treatment of

the unbounded region. The FEM-BEM method has been proposed by Silvester-Hsieh ([36]) and Zienkiewicz et al. ([40]), and analyzed by Johnson and Nedelec in [29] for the Laplace problem in the standard coupling procedure, that is when the finite computational domain is bounded internally by the physical obstacle and externally by an artificial boundary. In this case, the Dirichlet boundary conditions are enforced strongly, incorporating them directly in the approximation space.

The focus of this paper is twofold. First, we extend the results presented in [29] to the FEM-BEM fictitious domain method. As a typical example, we consider the Poisson equation, and we solve it in an enlarged domain that contains the obstacle, by imposing the homogeneous Dirichlet boundary condition weakly on the boundary of the obstacle (that turns out to be a curve internal to the enlarged domain). We prove existence, uniqueness and stability results for the solution of the variational problem by using the theory of saddle point problems. Moreover, we derive convergence results and error estimates for the standard Galerkin scheme.

The second aim of the paper is the study of waves propagating in infinite media and scattered by rotating rigid bodies. Possible applications are radar signals reflected by rotating aircraft propellers, TV and radio signals reflected by windmills, scattering of electromagnetic waves by moving plates. Boundary element methods seem difficult to apply to such problems and standard finite elements, coupled with NRBCs, would require the reconstruction, at each time step, of the mesh of the computational domain, which changes in time. Moreover, the change in mesh topology during the re-meshing would require the use of interpolation techniques to recover history variables on the newly generated mesh. This not only introduces artificial diffusivity, but it is also difficult and/or time-consuming to perform with sufficient robustness and accuracy. The FEM-BEM fictitious domain method represents an efficient alternative strategy. In case of moving bodies, in fact, the method has the great advantage of working with a given fixed mesh in the enlarged domain, thus avoiding the complexity of constructing at each time step a new finite element computational mesh. Furthermore, it requires only the construction of the discrete trace operator to enforce weakly the boundary conditions. In this case, the transmission conditions on the artificial boundary \mathcal{B} are imposed by a time-dependent boundary integral equation (see [16]).

For the numerical approximation of the proposed method, we present a full discretization by finite elements in space and a Crank-Nicolson time stepping scheme in the interior of the computational domain. For the discretization of the NRBC, we construct a numerical scheme which is based on a second order Lubich discrete convolution quadrature formula for the discretization of the time integral, coupled with a classical Galerkin (or collocation) method in space. Among the advantages of this transparent condition we recall the following ones: it allows the use of (smooth) curves of arbitrary shape for the choice of the artificial boundary; it can be used also in situations of multiple scattering; it allows the treatment of sources and initial data that must not be necessarily included in the finite computational domain; finally, its computational cost is much lower than what it might first appear, thanks to some special properties of the coefficients of the Lubich convolution quadratures. Indeed, if in the 2D case we choose a circular \mathcal{B} , the CPU required for the solution of some test problems is similar to that of local NBRCs.

Unfortunately, we do not have yet results concerning the analysis of the coupled FEM-

BEM fictitious domain approach for the time dependent wave equation, a task which is by no mean trivial. However, we refer the reader to [5] for the analysis of the standard FEM-BEM coupling for the 3D acoustic wave equation.

We remark that, for the treatment of rotating obstacles, an alternative approach consists of embedding the rotating body in a domain that rotates together with the scatterer. Such a domain is in turn placed inside a stationary residual domain (see, for example, [6] where a similar strategy is applied for the computation of flows induced by rotating components). By imposing the continuity of the discrete solution in a weak form on the interface between the rotating and the stationary subdomains, no compatible discretizations are required at the interface. With such an approach, no remeshing is required at each step of the time marching scheme. However, an interpolation technique is needed at each time step to recover the history of the solution on the rotated mesh. This would increase the computational overhead, especially when the discretization of the rotating domain must be chosen sufficiently fine to approximate accurately the boundary of the rotating scatterer.

The paper is organized as follows: in Section 2 we introduce the exterior elliptic model problem and the standard FEM-BEM formulation. The fictitious FEM-BEM approach, the existence of the solution and the stability of the corresponding saddle point formulation, as well as convergence and error estimates are presented in Sections 2.1, 2.2 and 2.3, respectively. In Sections 3 and 3.1 we present the exterior wave equation and the corresponding fictitious domain approach. In Section 3.2 we describe the full space-time discretization. Finally, numerical experiments are reported in Section 4, where we consider waves scattered by moving (even multiple) obstacles and non trivial external sources.

2 The Poisson problem

Let $\mathcal{O}^e = \mathbb{R}^2 \setminus \overline{\mathcal{O}}$ be the complement of a bounded rigid obstacle $\mathcal{O} \subset \mathbb{R}^2$, having a Lipschitz-continuous boundary Γ (see Figure 1, left plot). We consider the following exterior Dirichlet problem:

$$\begin{cases} -\Delta u(\mathbf{x}) &= f(\mathbf{x}), & \mathbf{x} \in \mathcal{O}^e \\ u(\mathbf{x}) &= 0, & \mathbf{x} \in \Gamma. \end{cases} \quad (1)$$

We assume that the source $f \in L^2(\mathcal{O}^e)$ has a compact support, which means that f is certainly null in a neighborhood of the boundary Γ , external to \mathcal{O} (hence the support of f does not cross Γ). We consider the asymptotic conditions

$$u(\mathbf{x}) = \alpha + O\left(\frac{1}{\|\mathbf{x}\|}\right) \quad \text{and} \quad \nabla u(\mathbf{x}) = O\left(\frac{1}{\|\mathbf{x}\|^2}\right) \quad \text{for} \quad \|\mathbf{x}\| \rightarrow \infty,$$

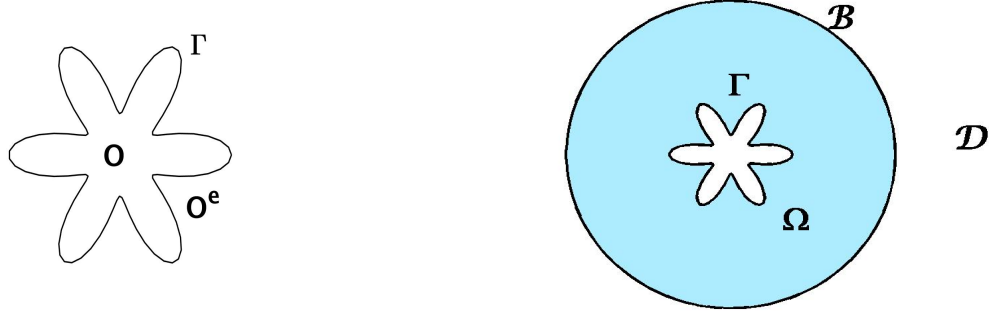
which guarantee the uniqueness of the solution in the space

$$W^1(\mathcal{O}^e) = \left\{ u : \left(\sqrt{1 + \|x\|^2} (1 + \log \sqrt{1 + \|x\|^2}) \right)^{-1} \cdot u \in L^2(\mathcal{O}^e), \nabla u \in [L^2(\mathcal{O}^e)]^2 \right\}$$

(see [29]).

To solve (1) by means of a finite element method, we truncate the infinite external domain by an artificial boundary \mathcal{B} , defined by a smooth curve. This boundary divides \mathcal{O}^e into two (open) sub-domains: a finite computational domain Ω , which is bounded internally by Γ and externally by \mathcal{B} , and an infinite residual domain \mathcal{D} (see Figure 1, right plot).

Figure 1: Geometry of the problem (left plot) and the finite computational domain Ω delimited by the artificial boundary \mathcal{B} (right plot).



We impose on \mathcal{B} the following NRBC (see [16, 19, 20])

$$\frac{1}{2}u(\mathbf{x}) = \mathcal{V}\partial_{\mathbf{n}_{\mathcal{D}}}u(\mathbf{x}) - \mathcal{K}u(\mathbf{x}) + I_f(\mathbf{x}) \quad \mathbf{x} \in \mathcal{B}, \quad (2)$$

where

$$\mathcal{V}\psi(\mathbf{x}) := \int_{\mathcal{B}} G(\mathbf{x} - \mathbf{y})\psi(\mathbf{y})d\mathcal{B}_{\mathbf{y}},$$

and

$$\mathcal{K}\varphi(\mathbf{x}) := \int_{\mathcal{B}} \partial_{\mathbf{n}_{\mathcal{D}}}G(\mathbf{x} - \mathbf{y})\varphi(\mathbf{y})d\mathcal{B}_{\mathbf{y}},$$

are the single and double layer integral operators. The function

$$G(\mathbf{x}) = -\frac{1}{2}\pi \log(\|\mathbf{x}\|)$$

is the fundamental solution of the Laplace equation $-\Delta u = 0$ and $\partial_{\mathbf{n}_{\mathcal{D}}}u$ denotes the outward normal derivative on $\mathcal{B} = \partial\mathcal{D}$. Incidentally, we remark that (2) is the trace on \mathcal{B} of the Kirchhoff's formula $u(\mathbf{x}) = \mathcal{V}\partial_{\mathbf{n}_{\mathcal{D}}}u(\mathbf{x}) - \mathcal{K}u(\mathbf{x}) + I_f(\mathbf{x})$, $\mathbf{x} \in \mathcal{D}$ (see [4]).

We assume that the artificial boundary \mathcal{B} is chosen in such a way that the support of f is included either in Ω or in \mathcal{D} , which means that the function f is null in a whole (two-sided) neighborhood of the boundary \mathcal{B} . The term

$$I_f(\mathbf{x}) = \int_{\mathcal{D}} f(\mathbf{y})G(\mathbf{x} - \mathbf{y})d\mathbf{y} \quad (3)$$

is the “volume” integral generated by the source f . In particular, it is non-trivial if the support of f is included in the infinite residual domain \mathcal{D} .

Setting $\lambda_{\mathcal{B}}(\mathbf{x}) = \partial_{\mathbf{n}_{\mathcal{D}}}u(\mathbf{x})$ and imposing the strong continuity of the solution u and of its normal derivative on \mathcal{B} , for the coupling of (1) and (2) (see [17]), we consider the new problem in the finite computational domain Ω :

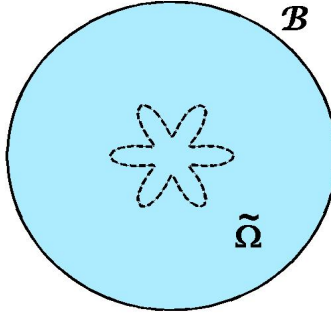
$$\begin{cases} -\Delta u(\mathbf{x}) & = f(\mathbf{x}) & \text{in } \Omega \\ u(\mathbf{x}) & = 0 & \text{on } \Gamma \\ \frac{1}{2}u(\mathbf{x}) - \boldsymbol{\nu}\lambda_{\mathcal{B}}(\mathbf{x}) + \boldsymbol{\kappa}u(\mathbf{x}) & = I_f(\mathbf{x}) & \text{on } \mathcal{B} \end{cases} \quad (4)$$

Note that f is non-trivial if the support of f is included in Ω . In the following sections we describe the FEM-BEM coupling method by using the fictitious domain approach for the solution of Problem (4).

2.1 The fictitious domain-Lagrange multiplier formulation

The fictitious domain method consists in extending artificially the solution of Problem (4) inside the obstacle, and in solving the new problem in the extended domain $\tilde{\Omega} := \Omega \cup \overline{\mathcal{O}}$, which is bounded by the artificial boundary \mathcal{B} (see Figure 2). In order to separate the numerical treatment of the differential operator from the one involving the boundary Γ , we enforce the Dirichlet boundary conditions on Γ by Lagrange multipliers. The main advantage of this approach is the possibility of solving the problem in a simpler domain and of choosing a mesh in the enlarged domain independent of the geometry of the obstacle.

Figure 2: The fictitious domain approach.



For the description of the method we restrict, for simplicity, to the case $I_f = 0$, and for this we assume that the support of the source term f is included in the finite computational domain $\tilde{\Omega}$ rather than in the residual domain \mathcal{D} . The case $I_f \neq 0$ implies the addition of a suitable right hand side term, which does not modify the forthcoming analysis.

For a generic function w defined in $\tilde{\Omega}$, we denote by $\gamma_{\Gamma}w$ and $\gamma_{\mathcal{B}}w$ its trace on Γ and on \mathcal{B} , respectively. For any $w \in H^1(\tilde{\Omega})$, it is known that its trace $\gamma_{\Gamma}w$ (resp. $\gamma_{\mathcal{B}}w$) belongs to $H^{1/2}(\Gamma)$ (resp. $H^{1/2}(\mathcal{B})$). We denote by $H^{-1/2}(\Gamma)$ (resp. $H^{-1/2}(\mathcal{B})$) the dual space of $H^{1/2}(\Gamma)$ (resp. $H^{1/2}(\mathcal{B})$). Moreover, for notational simplicity, we denote by f the extension of $f \in (H^1(\Omega))'$ to $\tilde{\Omega}$. Then, recalling the regularity properties of the boundary operators

\mathbf{V} and \mathbf{K} (see [35], Section 3.1.2), the variational formulation of Problem (4) reads: find $(u, \lambda_\Gamma, \lambda_\mathcal{B}) \in H^1(\tilde{\Omega}) \times H^{-1/2}(\Gamma) \times H^{-1/2}(\mathcal{B})$ such that

$$\begin{cases} a(u, v) + \langle \lambda_\Gamma, \gamma_\Gamma v \rangle_\Gamma + \langle \lambda_\mathcal{B}, \gamma_\mathcal{B} v \rangle_\mathcal{B} &= (f, v)_{\tilde{\Omega}} \quad \forall v \in H^1(\tilde{\Omega}), \\ \langle \varphi, \gamma_\Gamma u \rangle_\Gamma &= 0 \quad \forall \varphi \in H^{-1/2}(\Gamma) \\ 2\langle \mu, \mathbf{V} \lambda_\mathcal{B} \rangle_\mathcal{B} - \langle \mu, \gamma_\mathcal{B} u \rangle_\mathcal{B} - 2\langle \mu, \mathbf{K} \gamma_\mathcal{B} u \rangle_\mathcal{B} &= 0 \quad \forall \mu \in H^{-1/2}(\mathcal{B}). \end{cases} \quad (5)$$

where $a : H^1(\tilde{\Omega}) \times H^1(\tilde{\Omega}) \rightarrow \mathbb{R}$ is the bilinear form

$$a(v, w) = \int_{\tilde{\Omega}} \nabla v(\mathbf{x}) \cdot \nabla w(\mathbf{x}) d\mathbf{x}, \quad (6)$$

and $(v, w)_{\tilde{\Omega}} = \int_{\tilde{\Omega}} v(\mathbf{x}) w(\mathbf{x}) d\mathbf{x}$ denotes the L^2 scalar product. The bilinear forms $\langle \cdot, \cdot \rangle_\Gamma$ and $\langle \cdot, \cdot \rangle_\mathcal{B}$ denote the duality pairing between $H^{-1/2}(\Gamma)$ and $H^{1/2}(\Gamma)$, and $H^{-1/2}(\mathcal{B})$ and $H^{1/2}(\mathcal{B})$, respectively.

2.2 Existence results and stability analysis

The FEM-BEM coupling has been proposed in [36] and [40], and analyzed in [29] for the solution of the Laplace equation. Here we will analyze the coupling method in the fictitious domain approach. We remark that, the difference between our approach and the above mentioned one, consists in the fact that we seek the solution in the whole enlarged domain $\tilde{\Omega}$, while in the mentioned papers the problem is solved in the effective computational domain Ω . Hence, we impose the homogenous Dirichlet boundary conditions weakly on the (internal) closed curve Γ , by using Lagrange multipliers, rather than in imposing them strongly on Γ (the internal boundary of Ω), by inserting them directly into the variational formulation. Our approach leads to a saddle point formulation, for which existence results and stability analysis must be provided. In what follows we analyze the proposed method, by using known properties of the boundary integral operators that appear in the definition of the NRBC.

Following [29], we introduce the notations

$$H_\mathcal{B} := \left\{ \mu \in H^{-1/2}(\mathcal{B}) : \int_{\mathcal{B}} \mu = 0 \right\}, \quad V := H^1(\tilde{\Omega}) \times H_\mathcal{B},$$

and $\hat{u} = (u, \lambda_\mathcal{B}), \hat{v} = (v, \mu) \in V$. We consider the bilinear forms $B, K, A : V \times V \rightarrow \mathbb{R}$ defined by

$$\begin{aligned} B(\hat{u}, \hat{v}) &:= a(u, v) + \langle \lambda_\mathcal{B}, \gamma_\mathcal{B} v \rangle_\mathcal{B} + 2\langle \mu, \mathbf{V} \lambda_\mathcal{B} \rangle_\mathcal{B} - \langle \mu, \gamma_\mathcal{B} u \rangle_\mathcal{B}, \\ K(\hat{u}, \hat{v}) &:= 2\langle \mu, \mathbf{K} \gamma_\mathcal{B} u \rangle_\mathcal{B}, \quad A := B - K. \end{aligned}$$

The corresponding continuous linear operators are $B, K, A : V \rightarrow V'$ (for simplicity, they are defined using the same symbols of the bilinear forms), and are defined by

$$\langle B\hat{u}, \hat{v} \rangle_{V \times V'} = B(\hat{u}, \hat{v}), \quad \langle K\hat{u}, \hat{v} \rangle_{V \times V'} = K(\hat{u}, \hat{v}), \quad \langle A\hat{u}, \hat{v} \rangle_{V \times V'} = A(\hat{u}, \hat{v}),$$

where $\langle \cdot, \cdot \rangle_{V \times V'}$ denotes the duality product between V and its dual V' .

Setting $\hat{\lambda}_\Gamma = (\lambda_\Gamma, 0)$, $\hat{\varphi} = (\varphi, 0)$, $\hat{f} = (f, 0)$, and introducing the bilinear form

$$b_\Gamma(\hat{\lambda}_\Gamma, \hat{v}) := \langle \lambda_\Gamma, \gamma_\Gamma v \rangle_\Gamma,$$

Problem (5) can be reformulated in the following saddle point form: find $\hat{u} \in V$ and $\hat{\lambda}_\Gamma$, with $\lambda_\Gamma \in H^{-1/2}(\Gamma)$ such that

$$\begin{cases} A(\hat{u}, \hat{v}) + b_\Gamma(\hat{\lambda}_\Gamma, \hat{v}) &= (\hat{f}, \hat{v})_{\tilde{\Omega}} \quad \forall \hat{v} \in V, \\ b_\Gamma(\hat{\varphi}, \hat{u}) &= 0 \quad \forall \hat{\varphi} : \varphi \in H^{-1/2}(\Gamma). \end{cases} \quad (7)$$

Existence and uniqueness of the solution of (7) is strictly related to existence and uniqueness of the solution of the following problem

$$\begin{cases} B(\hat{u}, \hat{v}) + b_\Gamma(\hat{\lambda}_\Gamma, \hat{v}) &= (\hat{f}, \hat{v})_{\tilde{\Omega}} \quad \forall \hat{v} \in V, \\ b_\Gamma(\hat{\varphi}, \hat{u}) &= 0 \quad \forall \hat{\varphi}, \varphi \in H^{-1/2}(\Gamma). \end{cases} \quad (8)$$

In fact, (7) and (8) differ from each other only by a compact bilinear form (see [29]). Therefore, we first prove that Problem (8) admits a unique solution.

In the following, the notation $Q_1 \lesssim Q_2$ (resp. $Q_1 \gtrsim Q_2$) means that the quantity Q_1 is bounded from above (resp. from below) by $C \cdot Q_2$, where C is a constant that does not depend on Q_1 and Q_2 . Denoting by $\|\cdot\|_V$ the norm on the product space V defined as

$$\|\hat{v}\|_V := \sqrt{\|v\|_{H^1(\tilde{\Omega})}^2 + \|\mu\|_{H^{-1/2}(\mathcal{B})}^2},$$

the following result holds.

Theorem 2.1. *Problem (8) has a unique solution. Moreover, the following stability estimate holds:*

$$\|\hat{u}\|_V + \|\hat{\lambda}_\Gamma\|_{H^{-1/2}(\Gamma)} \lesssim \|\hat{f}\|_{V'}. \quad (9)$$

Proof. We note that the bilinear form $a(\cdot, \cdot)$ is continuous on $H^1(\tilde{\Omega})$ and that, by the trace theorem, $|\langle \lambda_\mathcal{B}, \gamma_\mathcal{B} v \rangle_\mathcal{B}|^2 \leq \|\gamma_\mathcal{B} v\|_{H^{1/2}(\mathcal{B})}^2 \|\lambda_\mathcal{B}\|_{H^{-1/2}(\mathcal{B})}^2 \lesssim \|v\|_{H^1(\tilde{\Omega})}^2 \|\lambda_\mathcal{B}\|_{H^{-1/2}(\mathcal{B})}^2$. Moreover (see [29]) the bilinear form

$$b_\mathcal{B} : H^{-1/2}(\mathcal{B}) \times H^{-1/2}(\mathcal{B}) \rightarrow \mathbb{R}, \quad b_\mathcal{B}(\lambda_\mathcal{B}, \mu) := \langle \mu, \boldsymbol{\nu} \lambda_\mathcal{B} \rangle_\mathcal{B}$$

is continuous. This ensures the continuity of the bilinear form B , namely $|B(\hat{u}, \hat{v})| \lesssim \|\hat{u}\|_V \|\hat{v}\|_V$.

Let us now define the kernel

$$\text{Ker}(b_\Gamma) := \{\hat{v} \in V : \langle \varphi, \gamma_\Gamma v \rangle_\Gamma = 0, \forall \varphi \in H^{-1/2}(\Gamma)\}.$$

It is easy to prove that $\text{Ker}(b_\Gamma) \equiv H_{0,\Gamma}^1(\tilde{\Omega}) \times H_\mathcal{B}$, where $H_{0,\Gamma}^1(\tilde{\Omega}) = \{v \in H^1(\tilde{\Omega}) : \gamma_\Gamma v = 0 \text{ on } \Gamma\}$. The operator $\boldsymbol{\nu}$ is known to be elliptic (see [29]), that is, there exists $\beta > 0$ such that:

$$\langle \mu, \boldsymbol{\nu} \mu \rangle_\mathcal{B} \geq \beta \|\mu\|_{H^{-1/2}(\mathcal{B})}^2, \quad \forall \mu \in H_\mathcal{B}. \quad (10)$$

Hence, from (10), and using the coercivity of the bilinear form $a(\cdot, \cdot)$ on $H_{0,\Gamma}^1(\tilde{\Omega})$ (see [11]), it follows that, for all $\hat{v}_0 = (v_0, \mu) \in \text{Ker}(b_\Gamma)$, we have

$$\begin{aligned} B(\hat{v}_0, \hat{v}_0) &= a(v_0, v_0) + \langle \mu, \gamma_\Gamma v_0 \rangle_{\mathcal{B}} - \langle \mu, \gamma_\Gamma v_0 \rangle_{\mathcal{B}} + 2\langle \mu, \mathbf{V}\mu \rangle_{\mathcal{B}} \\ &\geq \alpha_0 \|v_0\|_{H^1(\tilde{\Omega})}^2 + 2\beta \|\mu\|_{H^{-1/2}(\mathcal{B})}^2 \gtrsim \|\hat{v}_0\|_V^2, \end{aligned}$$

that is, B is coercive on $\text{Ker}(b_\Gamma)$. Moreover, the following inf-sup condition holds (see [21]):

$$\inf_{\varphi \in H^{-1/2}(\Gamma)} \sup_{v \in H^1(\tilde{\Omega})} \frac{\langle \varphi, \gamma_\Gamma v \rangle_\Gamma}{\|\varphi\|_{H^{-1/2}(\Gamma)} \|v\|_{H^1(\tilde{\Omega})}} = C > 0. \quad (11)$$

Therefore, according to the theory of saddle point problems (see [9]), and to the surjectivity of the trace operator γ_Γ , we can conclude that Problem (8) admits a unique solution $(\hat{u}, \hat{\lambda}_\Gamma)$. The stability estimate (9) directly follows (see [9]). \square

Theorem 2.1 states that the operator $B : V \rightarrow V'$ is invertible on $\text{Ker}(b_\Gamma)$. Since $A = B - K$, Problem (7) can be rewritten as follows: find $(\hat{u}, \hat{\lambda}_\Gamma) \in \text{Ker}(b_\Gamma)$ such that

$$(I - B^{-1}K)(\hat{u})(\hat{v}) = (B^{-1}\hat{f})(\hat{v}) \quad \forall \hat{v} \in \text{Ker}(b_\Gamma). \quad (12)$$

In [29] (Lemma 1 and following remarks), the authors prove that, setting $H_{0,\Gamma}^1(\Omega) = \{w \in H^1(\Omega) : \gamma_\Gamma w = 0 \text{ on } \Gamma\}$, the operator $B^{-1}K : H_{0,\Gamma}^1(\Omega) \times H_{\mathcal{B}} \rightarrow H^2(\Omega) \times H^{1/2}(\mathcal{B})$ is continuous. Moreover, since $H^2(\Omega) \times H^{1/2}(\mathcal{B})$ is compactly embedded in $H_{0,\Gamma}^1(\Omega) \times H_{\mathcal{B}}$, the operator $B^{-1}K : H_{0,\Gamma}^1(\Omega) \times H_{\mathcal{B}} \rightarrow H_{0,\Gamma}^1(\Omega) \times H_{\mathcal{B}}$ is compact.

Replacing $H_{0,\Gamma}^1(\Omega)$ by $H_{0,\Gamma}^1(\tilde{\Omega})$ and $H^2(\Omega)$ by $H^2(\tilde{\Omega})$, and noting that in our case Γ is a (closed) regular curve included in $\tilde{\Omega}$ rather than the internal boundary of the computational physical domain Ω , similarly to [29] we can prove that the operator $B^{-1}K : H_{0,\Gamma}^1(\tilde{\Omega}) \times H_{\mathcal{B}} \rightarrow H_{0,\Gamma}^1(\tilde{\Omega}) \times H_{\mathcal{B}}$ is compact. According to the remark that $\text{Ker}(b_\Gamma) \equiv H_{0,\Gamma}^1(\tilde{\Omega}) \times H_{\mathcal{B}}$, we conclude that $B^{-1}K : \text{Ker}(b_\Gamma) \rightarrow \text{Ker}(b_\Gamma)$ is compact and hence (12) is a second kind Fredholm equation. Therefore, for the existence of a solution of (12), it is sufficient to prove the following uniqueness result, whose proof can be found, again, in [29].

Lemma 2.2. *There exists only one $\hat{u} \in \text{Ker}(b_\Gamma)$ such that $A\hat{u} = \hat{f}$. Moreover $A : V \rightarrow V'$ is invertible on $\text{Ker}(b_\Gamma)$.*

We summarize the global result in the following Theorem (see [9]):

Theorem 2.3. *The operator $A : V \rightarrow V'$ is continuous and invertible on $\text{Ker}(b_\Gamma)$; furthermore, the continuous linear form $b_\Gamma : V \rightarrow (H^{-1/2}(\Gamma))'$ satisfies the inf-sup condition (11). Thus, Problem (7) admits a unique solution $(\hat{u}, \hat{\lambda}_\Gamma)$ that satisfies the stability bound (9).*

2.3 Approximation and error estimates

We consider a decomposition of $\tilde{\Omega} \approx \tilde{\Omega}_\Delta = \cup_{K_i \in \mathcal{T}_h} K_i$ into triangular elements. We assume that the mesh is quasi-uniform and we denote by h the spatial mesh size of the decomposition, defined as

$$h = \max_{K_i \in \mathcal{T}_h} h_{K_i},$$

where h_{K_i} denotes the diameter of the triangle K_i . For the approximation of $H^1(\tilde{\Omega})$, we introduce the finite dimensional space

$$X_h = \{v_h \in C^0(\tilde{\Omega}) : v_{h|_{K_i}} \in \mathbb{P}^k(K_i), K_i \in \mathcal{T}_h\},$$

where \mathbb{P}^k denotes the space of polynomials of degree $k \geq 1$. We assume that the curve Γ is given by a smooth parametric representation. In this case, we consider a partitioning of Γ into curvilinear elements $\Gamma = \cup_{i=1}^{M_\Gamma} S_i$, where M_Γ denotes the number of subintervals of the parametrization interval. Denoting by δ the maximum mesh size on Γ , we define

$$\Phi_\delta = \{\varphi_\delta : \varphi_{\delta|_{S_i}} \in \mathbb{P}^{k-1}(S_i), S_i \in \Gamma\} \subset H^{-1/2}(\Gamma),$$

the finite dimensional subspace of $H^{-1/2}(\Gamma)$ of piecewise polynomials of degree $k-1$, with respect to the curvilinear abscissas, on every S_i . Note that the discretization of the Lagrange multipliers is a priori completely independent of the trial space X_h . Moreover, since the Lagrange multiplier λ_Γ plays the role of the normal derivative of the solution along Γ , it is natural to approximate it by means of polynomials of local degree $k-1$. We also assume that the artificial boundary \mathcal{B} is given by a smooth parametric representation. Hence, we decompose the artificial boundary \mathcal{B} into curvilinear elements $\mathcal{B} = \cup_{i=1}^{M_\mathcal{B}} \mathcal{B}_i$, where $M_\mathcal{B}$ denotes the number of subintervals of the parametrization interval. In this case, the nodes defined on \mathcal{B} are those inherited by the triangulation of the entire domain $\tilde{\Omega}$ (see Figure 3, right plot). Therefore, we define

$$W_h = \{\psi_h : \psi_{h|\mathcal{B}_i} \in \mathbb{P}^k(\mathcal{B}_i), \mathcal{B}_i \in \mathcal{B}\} \subset H^{-1/2}(\mathcal{B}),$$

the finite dimensional subspace of $H^{-1/2}(\mathcal{B})$ of continuous piecewise polynomials of degree k , with respect to the curvilinear abscissas, defined on the mesh induced by the triangular decomposition of $\tilde{\Omega}$ on \mathcal{B} . We remark that, since the unknown $\lambda_\mathcal{B}$ represents the normal derivative on \mathcal{B} of the solution, the discrete space W_h could be chosen as the space of polynomials (not necessarily continuous) of degree $k-1$. However, as already remarked in [16], since the role of the NRBC is to define on \mathcal{B} a relationship between the (outgoing/incoming) wave and its normal derivative, which prevents the raising of spurious incoming/outgoing waves, the more accurate is the discretized relationship the more transparent this will be. To this end, we use the same degree for the polynomial approximation of the unknown u as well as of $\lambda_\mathcal{B}$.

The discrete spaces satisfy the following well known approximation properties:
for any $v \in H^s(\tilde{\Omega})$ with $2 \leq s \leq k+1$

$$\inf_{v_h \in X_h} \|v - v_h\|_{H^1(\tilde{\Omega})} \lesssim h^{s-1} \|v\|_{H^s(\tilde{\Omega})}; \quad (13)$$

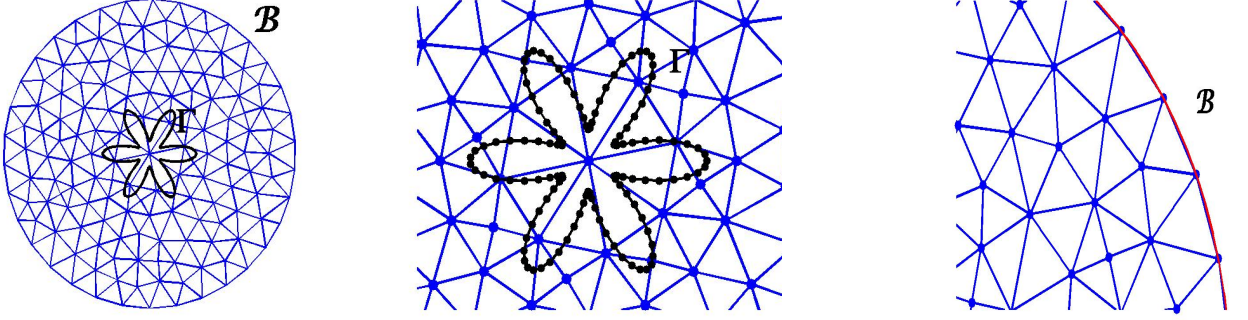
for any $\varphi \in H^r(\Gamma)$ with $-1/2 \leq r \leq k$

$$\inf_{\varphi_\delta \in \Phi_\delta} \|\varphi - \varphi_\delta\|_{H^{-1/2}(\Gamma)} \lesssim \delta^{r+1/2} \|\varphi\|_{H^r(\Gamma)}; \quad (14)$$

for any $\psi \in H^r(\mathcal{B})$ with $-1/2 \leq r \leq k+1$

$$\inf_{\psi_h \in W_h} \|\psi - \psi_h\|_{H^{-1/2}(\mathcal{B})} \lesssim h^{r+1/2} \|\psi\|_{H^r(\mathcal{B})}. \quad (15)$$

Figure 3: The meshes of the enlarged domain $\tilde{\Omega}$ and of the boundaries Γ and \mathcal{B} .



We refer to [34] for the approximation estimates with negative indexes (14) and (15), that are obtained by standard duality arguments.

Denoting by $V_h := X_h \times W_h \subset V$, we consider the discrete problem:

find $\hat{u}_h = (u_h, \lambda_{\mathcal{B},h}) \in V_h$ and $\hat{\lambda}_{\Gamma,\delta} = (\lambda_{\Gamma,\delta}, 0)$, $\lambda_{\Gamma,\delta} \in \Phi_\delta$ such that

$$\begin{cases} A(\hat{u}_h, \hat{v}_h) + b_\Gamma(\hat{\lambda}_{\Gamma,\delta}, \hat{v}_h) = (\hat{f}, \hat{v}_h)_{\tilde{\Omega}} & \forall \hat{v}_h \in V_h, \\ b_\Gamma(\hat{\varphi}_\delta, \hat{u}_h) = 0 & \forall \hat{\varphi}_\delta = (\varphi_\delta, 0), \varphi_\delta \in \Phi_\delta. \end{cases} \quad (16)$$

To prove existence and uniqueness of the solution of (16) we first establish some preliminary results. We denote by

$$\text{Ker}(b_{\Gamma,h}) = \{\hat{v}_h \in V_h : \langle \varphi_\delta, \gamma_\Gamma v_h \rangle_\Gamma = 0, \forall \varphi_\delta \in \Phi_\delta\}.$$

Remark 2.4. Since Φ_δ contains the constant functions, it follows that a function $\hat{u}_h \in \text{Ker}(b_{\Gamma,h})$ satisfies $\int_\Gamma u_h = 0$.

Lemma 2.5. For all $u \in H^1(\tilde{\Omega})$ such that $\int_\Gamma u = 0$, the following Poincaré inequality holds (see [39]):

$$\|u\|_{L^2(\tilde{\Omega})} \leq C \|\nabla u\|_{L^2(\tilde{\Omega})},$$

where C is a constant that depends only on $\tilde{\Omega}$.

Lemma 2.6. The bilinear form $a(\cdot, \cdot)$ is coercive on $\text{Ker}(b_{\Gamma,h})$, that is

$$a(u_h, u_h) \gtrsim \|u_h\|_{1,\tilde{\Omega}}^2 \quad \forall u_h \in \text{Ker}(b_{\Gamma,h}).$$

Proof. The proof immediately follows from Remark 2.4 and Lemma 2.5. \square

Lemma 2.7. Suppose that the spaces X_h and Φ_δ are chosen in such a way that there exists a constant β such that $\delta > \beta h$. Then the following uniform discrete inf-sup condition holds:

$$\inf_{\varphi \in \Phi_\delta} \sup_{v \in X_h} \frac{\langle \varphi, \gamma_\Gamma v \rangle_\Gamma}{\|\varphi\|_{H^{-1/2}(\Gamma)} \|v\|_{H^1(\tilde{\Omega})}} = C > 0. \quad (17)$$

Remark 2.8. *The inf-sup condition (17) states that a compatibility relation, between the triangular mesh defined on $\tilde{\Omega}$ and the mesh defined on Γ , must be satisfied. This means that the two meshes can not be chosen completely independent one from each other. In [21], where uniform structured triangular grids are used, the value of the constant β is 3. For what concerns more generic quasi-uniform grids, the result holds for a constant β that depends, among other factors, on the regularity of the grid. For major details, we refer to [14], where the validity of the Ladyzhenskaya-Babuska-Brezzi (LBB or inf-sup) condition (17) is proved for discretized second order elliptic boundary value problems. There, as here, the boundary conditions are enforced by using Lagrange multipliers.*

We remark that, in all the performed numerical tests, we have noticed that the factor β is slightly larger than one.

The following Corollary, concerning the convergence of the FEM-BEM approximation of the solution of Problem (5), is an immediate consequence of Lemma 2.6 and of the discrete inf-sup condition (17).

Corollary 2.9. *Let $(\hat{u}, \lambda_\Gamma) \in V \times H^{-1/2}(\Gamma)$ be the solution of (5). Under the condition of Lemma 2.7, there exists one and only one solution $(\hat{u}_h, \lambda_{\Gamma,\delta}) \in V_h \times \Phi_\delta$ of (16) such that the following error estimate holds*

$$\|\hat{u} - \hat{u}_h\|_V + \|\lambda_\Gamma - \lambda_{\Gamma,\delta}\|_{H^{-1/2}(\Gamma)} \lesssim \left(\inf_{\hat{v}_h \in V_h} \|\hat{u} - \hat{v}_h\|_V + \inf_{\mu_\delta \in \Phi_\delta} \|\lambda_\Gamma - \mu_\delta\|_{H^{-1/2}(\Gamma)} \right).$$

Before showing the error estimate let us make some remarks on the smoothness of the solution $(\hat{u}, \lambda_\Gamma)$ of equation (5). Assume that $f \in H^{s-2}(\tilde{\Omega})$ for some $s \geq 2$. Then, it is not difficult to realize that $u|_\Omega \in H^s(\Omega)$ and $u|_\mathcal{O} \in H^s(\mathcal{O})$. However, unless we do not choose the extension to \mathcal{O} of the right hand side f in a compatible way with the Dirichlet boundary condition on Γ , we will not in general have $u \in H^s(\tilde{\Omega})$, since the normal derivative will jump across Γ . The maximum overall regularity that we can in general expect is $u \in H^t(\tilde{\Omega})$, for $t < 3/2$. On the other hand, since λ_Γ is the jump on Γ of the normal derivative of u , we will have that $\lambda_\Gamma \in H^{s-3/2}(\Gamma)$. Note that u will have an higher regularity if and only if $\lambda_\Gamma = 0$. In view of these observations, by standard arguments, we have the following error estimate.

Lemma 2.10. *Let $(\hat{u}, \lambda_\Gamma) \in V \times H^{-1/2}(\Gamma)$ be the solution of (5). Let us assume that $f \in H^{s-2}(\tilde{\Omega})$ with $2 \leq s \leq k+1$. Then the following error estimate holds for all $\epsilon > 0$*

$$\|\hat{u} - \hat{u}_h\|_V + \|\lambda_\Gamma - \lambda_{\Gamma,\delta}\|_{H^{-1/2}(\Gamma)} \lesssim h^{1/2-\epsilon} \|u\|_{H^{3/2-\epsilon}(\tilde{\Omega})} + h^{s-1} \|\lambda_\mathcal{B}\|_{H^{s-3/2}(\mathcal{B})} + \delta^{s-1} \|\lambda_\Gamma\|_{H^{s-3/2}(\Gamma)}.$$

Moreover, if the extension of the right hand side f is chosen in such a way that $u \in H^s(\tilde{\Omega})$, it holds

$$\|\hat{u} - \hat{u}_h\|_V + \|\lambda_\Gamma - \lambda_{\Gamma,\delta}\|_{H^{-1/2}(\Gamma)} \lesssim h^{s-1} \|u\|_{H^s(\tilde{\Omega})} + h^{s-1} \|\lambda_\mathcal{B}\|_{H^{s-3/2}(\mathcal{B})}.$$

Remark 2.11. *The choice of the extension f in such a way that it is compatible with the boundary conditions on Γ is far from being a trivial problem and has until now no satisfactory solution. As a consequence, the a priori error estimates for most fictitious domain methods suffer from the limitation deriving from the lack of regularity of the extended*

solution ($u \notin H^{3/2}(\tilde{\Omega})$). In order to overcome this limitation one could resort to more sophisticated methods in the fictitious domain class (see for instance [33], [8], [2]). These approaches are of course possible also in our framework, but their study is beyond the scope of this paper.

3 Waves scattered by rotating rigid bodies

In this section we extend the fictitious domain FEM-BEM coupling to the case of waves scattered by moving obstacles.

Let $\mathcal{O}^e(t) = \mathbb{R}^2 \setminus \overline{\mathcal{O}}(t)$ be the complement of a rotating bounded rigid obstacle $\mathcal{O}(t) \subset \mathbb{R}^2$, having a smooth boundary $\Gamma(t)$. We denote by \mathcal{O}_0^e the initial configuration of the obstacle at $t = 0$. We consider the following exterior model problem:

$$\begin{cases} u_{tt}(\mathbf{x}, t) - \Delta u(\mathbf{x}, t) &= f(\mathbf{x}, t) & \text{in } \mathcal{O}^e(t) \times (0, T) \\ u(\mathbf{x}, t) &= 0 & \text{in } \Gamma(t) \times (0, T) \\ u(\mathbf{x}, 0) &= u_0(\mathbf{x}) & \text{in } \mathcal{O}_0^e \\ u_t(\mathbf{x}, 0) &= v_0(\mathbf{x}) & \text{in } \mathcal{O}_0^e. \end{cases} \quad (18)$$

We assume that the data are smooth and satisfy the required compatibility conditions, which guarantee that the solution $u(\mathbf{x}, t)$ is at least C^2 with respect to both variables. That is, we assume (see [19]) $f \in C([0, T], C^2(\overline{\mathcal{O}^e(t)}))$, $u_0 \in C^3(\overline{\mathcal{O}_0^e})$, $v_0 \in C^2(\overline{\mathcal{O}_0^e})$. We also assume, as it often occurs in practical situations, that the initial data u_0, v_0 and the source term f have local supports; in particular, we assume that the functions u_0, v_0 are null in a neighborhood of the boundary $\Gamma_0 := \Gamma(t = 0)$, and that f is null in a neighborhood of the boundary $\Gamma(t)$ for all $t \in [0, T]$ (which implies that the support of f does not intersect the boundary $\Gamma(t)$ throughout the time). From these properties, we immediately deduce that $u(\mathbf{x}, 0) = u_t(\mathbf{x}, 0) = u_{tt}(\mathbf{x}, 0) = 0$ if $\mathbf{x} \in \Gamma_0$.

We choose a fixed artificial boundary \mathcal{B} , in such a way that the rotating obstacle is included in the region surrounded by \mathcal{B} in the whole time interval $[0, T]$. The finite computational domain, bounded internally by $\Gamma(t)$ and externally by \mathcal{B} , is denoted by $\Omega(t)$. On \mathcal{B} , we impose a time dependent NRBC.

Many time dependent NRBCs have been proposed in the last two-three decades, and most of them are local, both in time and space. For a review, see for example [22], [23], [24]. All these papers, except for [1], [37], [27], [28], [16], [5], deal with the construction of NRBC with the property of absorbing only outgoing waves, and not also the incoming ones. Therefore, the sources must necessarily be included in the computational domain, and this represents a severe drawback when, for example, sources are far away from the physical domain. Moreover, most of the local NRBCs works only for a single convex artificial boundary having a special shape, like a circle (sphere in 3D) or ellipse (ellipsoid in 3D).

We consider here the fully non local NRBC proposed in [16] (see also [17] and [18]). With abuse of notation, we denote by the same letters \mathcal{V} and \mathcal{K} used in Section 2 the time dependent single and double layer integral operators

$$\mathcal{V}\psi(\mathbf{x}, t) := \int_0^t \int_{\mathcal{B}} G(\mathbf{x} - \mathbf{y}, t - \tau) \psi(\mathbf{y}, \tau) d\mathcal{B}_{\mathbf{y}} d\tau,$$

and

$$\mathcal{K}\varphi(\mathbf{x}, t) := \int_0^t \int_{\mathcal{B}} \partial_{\mathbf{n}_{\mathcal{D}}} G(\mathbf{x} - \mathbf{y}, t - \tau) \varphi(\mathbf{y}, \tau) d\mathcal{B}_{\mathbf{y}} d\tau,$$

where

$$G(\mathbf{x}, t) = \frac{1}{2\pi} \frac{H(t - \|\mathbf{x}\|)}{\sqrt{t^2 - \|\mathbf{x}\|^2}}$$

is the fundamental solution of the wave equation (18) (being $H(\cdot)$ the Heaviside function). Then, we impose on \mathcal{B} the exact time dependent NRBC given by the following BIE:

$$\frac{1}{2}u(\mathbf{x}, t) = \mathcal{V}\partial_{\mathbf{n}_{\mathcal{D}}}u(\mathbf{x}, t) - \mathcal{K}u(\mathbf{x}, t) \quad \mathbf{x} \in \mathcal{B}. \quad (19)$$

Here we have assumed, for simplicity, that the supports of the data are included in $\Omega(t)$. In the case that these supports were included in $\mathcal{D} := \mathbb{R}^2 \setminus \overline{\Omega(t)} \cup \mathcal{O}(t)$, extra volume terms should be added to (19) (see [16]). With the above assumptions, the functions u_0, v_0, f are null in a whole (two-sided) \mathbb{R}^2 neighborhood of the boundary \mathcal{B} . This implies that $u(\mathbf{x}, 0) = \partial_{\mathbf{n}_{\mathcal{D}}}u(\mathbf{x}, 0) = 0$ if $\mathbf{x} \in \mathcal{B}$.

For convenience of the reader, we recall here the mapping properties of the operators \mathcal{V} and \mathcal{K} . We set $H_0^r(0, T) = \{h|_{(0, T)} : h \in H^r(\mathbb{R}) \text{ with } h \equiv 0 \text{ on } (-\infty, 0)\}$, where $H^r(\mathbb{R})$ denotes the classical Sobolev space of order r defined on the real line. When r is an integer, this space consists of those functions g whose r -th distributional derivative is in $L^2(0, T)$ and which have $h(0) = \dots h^{(r-1)}(0) = 0$. Then:

- $H_0^r(0, T; X)$ is the space of $H_0^r(0, T)$ functions of t , $\phi(\mathbf{x}, t)$, such that, setting $\phi(\mathbf{x}, t) = \phi(t)(\mathbf{x})$, we have $\phi(t) \in X$, with $\|\phi(t)\|_X \|_{H^r(0, T)} < \infty$.
- $H^{1/2}(\mathcal{B})$ and $H^{-1/2}(\mathcal{B})$ are the trace space on the artificial boundary, of $H^1(\Omega)$ functions, and the corresponding dual space, respectively.

Recalling that $u(\mathbf{x}, 0)$ and $\partial_{\mathbf{n}_{\mathcal{D}}}u(\mathbf{x}, 0)$, together with their first time derivatives, vanish at $t = 0$, we obtain (see also [31], p.368) the following mapping properties for the bounded operators \mathcal{V} and \mathcal{K} :

$$\mathcal{V} : H_0^{r+1}(0, T; H^{-1/2}(\mathcal{B})) \rightarrow H_0^r(0, T; H^{1/2}(\mathcal{B})), r \geq 0 \quad (20)$$

and

$$\mathcal{K} : H_0^{r+3/2}(0, T; H^{1/2}(\mathcal{B})) \rightarrow H_0^r(0, T; H^{1/2}(\mathcal{B})), r \geq 0. \quad (21)$$

Recalling the well known embedding property: $H^r(0, T) \subset C^m[0, T]$ for $r > m + 1/2$, from (20) and (21) we deduce that the assumption $r > 3/2$ guarantees that

$$\mathcal{V} : H_0^r(0, T; H^{-1/2}(\mathcal{B})) \rightarrow C([0, T]; H^{1/2}(\mathcal{B})).$$

Furthermore, if $r > 2$ we also have

$$\mathcal{K} : H_0^r(0, T; H^{1/2}(\mathcal{B})) \rightarrow C([0, T]; H^{1/2}(\mathcal{B})).$$

Here, $C(I; X)$ denotes the space of C^0 functions of $t \in I$, such that for each value of t the corresponding function of \mathbf{x} belongs to the space X .

Note that in our case we have $u \in H_0^r(0, T; H^r(\mathcal{B}))$, $\partial_{\mathbf{n}_D} u \in H_0^r(0, T; H^{r-1}(\mathcal{B}))$, where r is at least 2. This is a straight consequence of the assumptions we have made on the problem data. These assumptions also guarantee that all terms of our NRBC (19) are, in particular, continuous functions of $\mathbf{x} \in \mathcal{B}$. Thus, the NRBC it is well defined at any point of the boundary \mathcal{B} .

Setting $\lambda_{\mathcal{B}}(\mathbf{x}, t) = \partial_{\mathbf{n}_D} u(\mathbf{x}, t)$, the new problem in the finite computational domain $\Omega(t)$ reads:

$$\begin{cases} u_{tt}(\mathbf{x}, t) - \Delta u(\mathbf{x}, t) &= f(\mathbf{x}, t) & \text{in } \Omega(t) \times (0, T) \\ u(\mathbf{x}, t) &= 0 & \text{in } \Gamma(t) \times (0, T) \\ \frac{1}{2}u(\mathbf{x}, t) - \mathbf{V}\lambda_{\mathcal{B}}(\mathbf{x}, t) + \mathcal{K}u(\mathbf{x}, t) &= 0 & \text{in } \mathcal{B} \times (0, T) \\ u(\mathbf{x}, 0) &= u_0(\mathbf{x}) & \text{in } \Omega_0 \\ u_t(\mathbf{x}, 0) &= v_0(\mathbf{x}) & \text{in } \Omega_0, \end{cases} \quad (22)$$

where $\Omega_0 := \Omega(t = 0)$ is the initial configuration of the finite computational domain.

The application of a standard finite element method to Problem (22) is not a simple task; furthermore, this approach would, in any case, require the reconstruction of the computational mesh at each time step. To avoid such complexity, the fictitious domain approach seems to be a very attractive solution. Moreover, the main advantage of this approach, in the time dependent case, is the possibility of solving the problem in a simpler domain and of choosing a fixed mesh in the enlarged domain independent of the geometry of the obstacle (and hence of t), thus avoiding the complexity of constructing at each time step a new computational mesh.

It is worth mentioning here the recent papers [15] and [32], for the application of standard finite element methods to PDEs on evolving surfaces.

3.1 The fictitious domain approach

For a generic time dependent function w defined in $\tilde{\Omega}$, we set $w(t)(\mathbf{x}) := w(\mathbf{x}, t)$. Recalling the regularity properties (20) and (21) of the boundary operators \mathbf{V} and \mathcal{K} , the problem defined in the domain of interest $\tilde{\Omega}$ consists in the following weak formulation:

for any $t > 0$, given $f(t) \in (H^1(\tilde{\Omega}))'$, find the triad of unknown functions $(u(t), \lambda_{\Gamma}(t), \lambda_{\mathcal{B}}(t)) \in H^1(\tilde{\Omega}) \times H^{-1/2}(\Gamma(t)) \times H^{-1/2}(\mathcal{B})$ such that $\forall v \in H^1(\tilde{\Omega})$, $\forall \varphi(t) \in H^{-1/2}(\Gamma(t))$ and $\forall \mu \in$

$H^{-1/2}(\mathcal{B})$, the following generalized saddle-point evolution problem

$$\begin{cases} \frac{d^2}{dt^2}(u(t), v)_{\tilde{\Omega}} + a(u(t), v) + \langle \lambda_{\Gamma}(t), \gamma_{\Gamma(t)} v \rangle_{\Gamma(t)} + \langle \lambda_{\mathcal{B}}(t), \gamma_{\mathcal{B}} v \rangle_{\mathcal{B}} = (f(t), v)_{\tilde{\Omega}} & (23a) \\ \langle \varphi(t), \gamma_{\Gamma(t)} u(t) \rangle_{\Gamma(t)} = 0 & (23b) \\ 2\langle \mu, \mathbf{V} \lambda_{\mathcal{B}}(t) \rangle_{\mathcal{B}} - \langle \mu, \gamma_{\mathcal{B}} u(t) \rangle_{\mathcal{B}} - 2\langle \mu, \mathbf{K} \gamma_{\mathcal{B}} u(t) \rangle_{\mathcal{B}} = 0 & (23c) \\ u(0) = u_0 \quad \text{in } \tilde{\Omega} & (23d) \\ \frac{du}{dt}(0) = v_0 \quad \text{in } \tilde{\Omega} & (23e) \end{cases}$$

holds in the distributional sense in $(0, T)$, where $a(\cdot, \cdot)$ is defined in (6) and $\gamma_{\Gamma(t)}$ denotes the time dependent trace operator on $\Gamma(t)$. As we have already mentioned, this approach allows to decouple the differential operator from the boundary conditions so that the change of the boundary $\Gamma(t)$ with respect to time can be treated adequately by simply modifying the bilinear form $\langle \cdot, \cdot \rangle_{\Gamma(t)}$ that appears in (23a) and (23b). Moreover, for the numerical solution, the main amount of work, that is the mesh generation for the whole domain $\tilde{\Omega}$, the construction of the stiffness matrix associated to the bilinear form $a(\cdot, \cdot)$ and of the mass matrix associated to the L^2 scalar product, is performed once for all on a simpler domain. It is worth noting that the additional unknown function, namely the Lagrange multiplier $\lambda_{\Gamma}(t)$, turns out to be the normal derivative of u at $\Gamma(t)$ (see [3]).

As already mentioned, the analysis of the coupled problem (23) is still under study. In the next sections we present the full space-time discretization of (23) and several numerical tests that we have performed to validate the proposed scheme.

3.2 Full space-time formulation: approximation and implementation details

3.2.1 Discretization of the time dependent NRBC

We start by briefly recalling the main steps of the Lubich-Galerkin method for the discretization of the NRBC (23c), namely of the integral operators appearing in it (for more details we refer to [30] and [19]). We recall that equation (23c) represents the natural relation that u and its normal derivative have to satisfy on the artificial boundary \mathcal{B} at each time t , and that (23c) has not to be solved independently of the remaining equations of (23) (neither u nor $\lambda_{\mathcal{B}}$ are given on \mathcal{B}). The coupling of the discretization of this equation with the discretization of the full FEM-BEM fictitious method will be detailed in the next section.

The Lubich convolution quadrature formulas have the fundamental property of using the Laplace transform of the kernel of the integral equation they are applied to, instead of its explicit expression. In particular, the discretization in time is based on the splitting of the interval $[0, T]$ into N steps of equal length $\Delta_t = T/N$ and in the collocation of the equation (23c) at the discrete time levels $t_n = n\Delta_t$, $n = 0, \dots, N$.

The time integrals appearing in the definition of the single and double layer operators are discretized here by means of the convolution quadrature formula associated with the second

order Backward Differentiation Method (BDF) for ordinary differential equations (see [19] for details). In particular

$$\mathbf{V}\lambda_{\mathcal{B}}(\cdot, t_n) \approx \sum_{j=0}^n \int_{\mathcal{B}} \omega_{n-j}^{\mathbf{V}}(\Delta_t; \|\cdot - \mathbf{y}\|) \lambda_{\mathcal{B}}(\mathbf{y}, t_j) d\mathcal{B}_{\mathbf{y}}, \quad n = 0, \dots, N \quad (24)$$

$$\mathbf{K}\gamma_{\mathcal{B}}u(\cdot, t_n) \approx \sum_{j=0}^n \int_{\mathcal{B}} \omega_{n-j}^{\mathbf{K}}(\Delta_t; \|\cdot - \mathbf{y}\|) \gamma_{\mathcal{B}}u(\mathbf{y}, t_j) d\mathcal{B}_{\mathbf{y}}, \quad n = 0, \dots, N. \quad (25)$$

The coefficients $\omega_n^{\mathcal{J}}, \mathcal{J} = \mathbf{V}, \mathbf{K}$, are given by

$$\omega_n^{\mathcal{J}}(\Delta_t; \|\mathbf{x} - \mathbf{y}\|) = \frac{1}{2\pi i} \int_{|z|=\rho} K^{\mathcal{J}} \left(\|\mathbf{x} - \mathbf{y}\|, \frac{\gamma(z)}{\Delta_t} \right) z^{-(n+1)} dz, \quad (26)$$

where in this case $K^{\mathbf{V}} = \widehat{G}$ is the Laplace transform of the kernel G appearing in the definition of the single layer operator \mathbf{V} , and $K^{\mathbf{K}} = \widehat{\partial G / \partial \mathbf{n}}$ is the Laplace transform of $\partial G / \partial \mathbf{n}$ appearing in the double layer operator \mathbf{K} . In particular,

$$K^{\mathbf{V}}(r, s) = \frac{1}{2\pi} K_0(rs), \quad K^{\mathbf{K}}(r, s) = -\frac{1}{2\pi} s K_1(rs) \frac{\partial r}{\partial \mathbf{n}},$$

where $K_0(z)$ and $K_1(z)$ are the second kind modified Bessel functions of order 0 and 1, respectively. The function $\gamma(z) = 3/2 - 2z + 1/2z^2$ is the so called characteristic quotient of the BDF method of order 2. The parameter ρ is such that for $|z| \leq \rho$ the corresponding $\gamma(z)$ lies in the domain of analyticity of $K^{\mathcal{J}}$. Inserting (24) and (25) in (23c), we obtain the semi-discrete boundary integral relation

$$\begin{aligned} & 2 \sum_{j=0}^n \langle \mu, \int_{\mathcal{B}} \omega_{n-j}^{\mathbf{V}}(\Delta_t; \|\cdot - \mathbf{y}\|) \lambda_{\mathcal{B}}(\mathbf{y}, t_j) d\mathcal{B}_{\mathbf{y}} \rangle_{\mathcal{B}} - \langle \mu, \gamma_{\mathcal{B}}u(t_n) \rangle_{\mathcal{B}} \\ & - 2 \sum_{j=0}^n \langle \mu, \int_{\mathcal{B}} \omega_{n-j}^{\mathbf{K}}(\Delta_t; \|\cdot - \mathbf{y}\|) \gamma_{\mathcal{B}}u(\mathbf{y}, t_j) d\mathcal{B}_{\mathbf{y}} \rangle_{\mathcal{B}} = 0. \end{aligned} \quad (27)$$

For the space discretization of (27), recalling that we assume that the artificial boundary \mathcal{B} is given by a parametric representation, at each time instant t_j we approximate the unknown function $u(\mathbf{x}, t_j)$ on \mathcal{B} and its normal derivative $\lambda_{\mathcal{B}}(\mathbf{x}, t_j)$ by continuous piecewise linear interpolants (with respect to the curvilinear abscissas), defined on curvilinear elements and associated with the partition $\{\mathbf{x}_m, m = 1, \dots, M_{\mathcal{B}}\}$ into $M_{\mathcal{B}}$ segments, inherited on \mathcal{B} by the triangular decomposition $\widetilde{\Omega}_{\Delta}$. We remark that, as in the time independent case, this choice allows to have a discretization of the NRBC more accurate than the one obtained by choosing a piecewise constant approximation of $\lambda_{\mathcal{B}}$.

Therefore, denoting by $u_{\mathcal{B}}$ the trace of u on \mathcal{B} , $u_{\mathcal{B}} := \gamma_{\mathcal{B}}u$, at each time instant t_j the unknown functions $u_{\mathcal{B}}(\cdot, t_j)$ and $\lambda_{\mathcal{B}}(\cdot, t_j)$ are approximated by

$$u_{\mathcal{B},h}(\mathbf{x}, t_j) := \sum_{k=1}^{M_{\mathcal{B}}} u_{\mathcal{B},k}^j N_k^{\mathcal{B}}(\mathbf{x}) \quad \text{and} \quad \lambda_{\mathcal{B},h}(\mathbf{x}, t_j) := \sum_{k=1}^{M_{\mathcal{B}}} \lambda_{\mathcal{B},k}^j N_k^{\mathcal{B}}(\mathbf{x}) \quad (28)$$

where $u_{\mathcal{B},k}^j \approx u_{\mathcal{B}}(\mathbf{x}_k, t_j)$, $\lambda_{\mathcal{B},k}^j \approx \lambda_{\mathcal{B}}(\mathbf{x}_k, t_j)$ and $\{N_i^{\mathcal{B}}\}_{i=1}^{M_{\mathcal{B}}}$ is the basis of the space W_h , that is the set of the continuous piecewise linear basis functions defined on curvilinear elements and associated with the partition $\{\mathbf{x}_m\}_{m=1}^{M_{\mathcal{B}}}$. Replacing (28) into (27), we write the full (Galerkin) space-time discrete boundary integral relation as follows:

$$2 \sum_{j=0}^n \sum_{k=1}^{M_{\mathcal{B}}} (\mathbf{V}_{n-j})_{mk} \lambda_{\mathcal{B},k}^j - \sum_{k=1}^{M_{\mathcal{B}}} \mathbf{M}_{mk}^{\mathcal{B}} u_{\mathcal{B},k}^n - 2 \sum_{j=0}^n \sum_{k=1}^{M_{\mathcal{B}}} (\mathbf{K}_{n-j})_{mk} u_{\mathcal{B},k}^j = 0, \quad m, k = 1, \dots, M_{\mathcal{B}},$$

where the matrices \mathbf{V}_{n-j} and \mathbf{K}_{n-j} are given by

$$(\mathbf{V}_{n-j})_{mk} = \int_{\mathcal{B}} \int_{\mathcal{B}} \omega_{n-j}^{\mathcal{V}}(\Delta_t; \|\mathbf{x} - \mathbf{y}\|) N_k^{\mathcal{B}}(\mathbf{x}) N_m^{\mathcal{B}}(\mathbf{y}) d\mathcal{B}_{\mathbf{x}} d\mathcal{B}_{\mathbf{y}}, \quad m, k = 1, \dots, M_{\mathcal{B}},$$

$$(\mathbf{K}_{n-j})_{mk} = \int_{\mathcal{B}} \int_{\mathcal{B}} \omega_{n-j}^{\mathcal{K}}(\Delta_t; \|\mathbf{x} - \mathbf{y}\|) N_k^{\mathcal{B}}(\mathbf{x}) N_m^{\mathcal{B}}(\mathbf{y}) d\mathcal{B}_{\mathbf{x}} d\mathcal{B}_{\mathbf{y}}, \quad m, k = 1, \dots, M_{\mathcal{B}},$$

and

$$\mathbf{M}_{mk}^{\mathcal{B}} = \int_{\mathcal{B}} N_k^{\mathcal{B}}(\mathbf{y}) N_m^{\mathcal{B}}(\mathbf{y}) d\mathcal{B}_{\mathbf{y}}, \quad m, k = 1, \dots, M_{\mathcal{B}}.$$

The integration over \mathcal{B} is reduced to an equivalent integration over the parametrization interval. The absorbing condition at time t_n is then written in matrix notation as:

$$2\mathbf{V}_0 \boldsymbol{\lambda}_{\mathcal{B}}^n - (\mathbf{M}^{\mathcal{B}} + 2\mathbf{K}_0) \mathbf{u}_{\mathcal{B}}^n = 2 \sum_{j=0}^{n-1} \mathbf{K}_{n-j} \mathbf{u}_{\mathcal{B}}^j - 2 \sum_{j=0}^{n-1} \mathbf{V}_{n-j} \boldsymbol{\lambda}_{\mathcal{B}}^j, \quad n = 1, \dots, N, \quad (29)$$

in the unknown vectors $\mathbf{u}_{\mathcal{B}}^j = (u_{\mathcal{B},1}^j, \dots, u_{\mathcal{B},M_{\mathcal{B}}}^j)$ and $\boldsymbol{\lambda}_{\mathcal{B}}^j = (\lambda_{\mathcal{B},1}^j, \dots, \lambda_{\mathcal{B},M_{\mathcal{B}}}^j)$.

Since, in the numerical section, we will couple the FEM scheme also with the strong form of the NRBC, we describe here, for completeness, the expression of the NRBC in the spatial collocation case. By collocating the discretized equation (27) at the points $\mathbf{x}_m, m = 1, \dots, M_{\mathcal{B}}$, the generic element of the matrices \mathbf{V}_{n-j} and \mathbf{K}_{n-j} are defined by

$$\int_{\mathcal{B}} \omega_{n-j}^{\mathcal{V}}(\Delta_t; \|\mathbf{x}_m - \mathbf{y}\|) N_k^{\mathcal{B}}(\mathbf{y}) d\mathcal{B}_{\mathbf{y}} \text{ and } \int_{\mathcal{B}} \omega_{n-j}^{\mathcal{K}}(\Delta_t; \|\mathbf{x}_m - \mathbf{y}\|) N_k^{\mathcal{B}}(\mathbf{y}) d\mathcal{B}_{\mathbf{y}}, \quad m, k = 1, \dots, M_{\mathcal{B}},$$

respectively, and the collocation space-time NRBC takes the form (29), where the matrix $\mathbf{M}^{\mathcal{B}}$ is replaced by the (square) identity matrix of order $M_{\mathcal{B}}$.

We remark that the integrals in the expression (26) of the coefficients $\omega_n^{\mathcal{J}}$ of the quadrature formula are efficiently computed by using the trapezoidal rule with $L \geq N$ equal steps of length $2\pi/L$. Moreover, they are computed simultaneously by using the FFT algorithm, with $O(N \log N)$ flops (see [19] for details).

3.2.2 Finite element approximation and time discretization of the complete scheme

We now consider the discretization in space of the equations (23a) and (23b). By using the notations introduced in Section 2.3, we consider the discretization spaces X_h and W_h with

$k = 1$. In particular, X_h is the finite element space of piecewise linear continuous functions and W_h is the boundary element space of piecewise linear continuous functions. We denote by $\{N_i^{\tilde{\Omega}}\}_{i \in \mathfrak{S}}$ and $\{N_i^{\mathcal{B}}\}_{i \in \mathfrak{S}_{\mathcal{B}}}$ ($\mathfrak{S}_{\mathcal{B}} = \{1 \dots, M_{\mathcal{B}}\}$, see Section 3.2.1) the chosen basis functions for these spaces, respectively. Moreover, we introduce

$$\Phi_{\delta}(t) = \{\varphi_{\delta}(\cdot, t) : \varphi_{\delta}(\cdot, t)|_{S_i(t)} \in \mathbb{P}^0(S_i(t)), S_i(t) \in \Gamma(t)\}$$

the boundary element space of piecewise constant functions on a partition of the boundary $\Gamma(t) = \cup_{i=1}^{M_{\Gamma}} S_i(t)$ into curvilinear elements $S_i(t)$. We remark that, since the boundary $\Gamma(t)$ is only subject to a rotation, but does not modify its shape in time, it is reasonable to consider a fixed number M_{Γ} for its partitioning. As a consequence, each element $S_i(t)$ has a fixed length that does not change in time. The (time independent) parameter δ denotes the maximum mesh size on $\Gamma(t)$, as in the time independent case. We denote by $\{N_i^{\Gamma(t)}\}_{i \in \mathfrak{S}_{\Gamma}}$ ($\mathfrak{S}_{\Gamma} = \{1 \dots, M_{\Gamma}\}$) the chosen basis functions for the space $\Phi_{\delta}(t)$. The semi-discretized (in space) equations (23a) and (23b) read: find $u_h(\cdot, t) \in X_h$, $\lambda_{\Gamma, \delta}(\cdot, t) \in \Phi_{\delta}(t)$, $\lambda_{\mathcal{B}, h}(\cdot, t) \in W_h$ such that

$$\begin{cases} \frac{d^2}{dt^2}(u_h, w_h)_{\tilde{\Omega}} + a(u_h, w_h) - \langle \lambda_{\Gamma, \delta}, \gamma_{\Gamma(t)} w_h \rangle_{\Gamma(t)} - \langle \lambda_{\mathcal{B}, h}, \gamma_{\mathcal{B}} w_h \rangle_{\mathcal{B}} &= (f(t), w_h) \quad \forall w_h \in X_h \\ \langle \varphi_{\delta}, \gamma_{\Gamma(t)} u_h \rangle_{\Gamma(t)} &= 0 \quad \forall \varphi_{\delta} \in \Phi_{\delta}(t). \end{cases}$$

Denoting by \mathbf{u} the (time dependent) unknown vector of the nodal values at the vertices of the triangularization of $\tilde{\Omega}$, and by $\boldsymbol{\lambda}_{\Gamma}$ and $\boldsymbol{\lambda}_{\mathcal{B}}$ the (time dependent) unknown vectors whose components represent the unknown values of the approximants of λ_{Γ} and $\lambda_{\mathcal{B}}$ associated with the nodes defined on $\Gamma(t)$ and \mathcal{B} respectively, we obtain the following system of ordinary differential equations

$$\begin{cases} \mathbf{M}^{\mathbf{F}} \ddot{\mathbf{u}} + \mathbf{A}^{\mathbf{F}} \mathbf{u} - \mathbf{B}(t) \boldsymbol{\lambda}_{\Gamma} - \mathbf{Q} \boldsymbol{\lambda}_{\mathcal{B}} &= \mathbf{f} \\ \mathbf{B}^T(t) \mathbf{u} &= \mathbf{0}. \end{cases} \quad (30)$$

The (square) matrices $\mathbf{M}^{\mathbf{F}}$ and $\mathbf{A}^{\mathbf{F}}$ are the mass and stiffness matrices associated to the L^2 -scalar product of the basis functions $\{N_i^{\tilde{\Omega}}\}_{i \in \mathfrak{S}}$ of X_h and to the bilinear form $a(N_i^{\tilde{\Omega}}, N_j^{\tilde{\Omega}})$, respectively:

$$\mathbf{M}^{\mathbf{F}}_{ij} = \int_{\tilde{\Omega}} N_i^{\tilde{\Omega}}(\mathbf{x}) N_j^{\tilde{\Omega}}(\mathbf{x}) d\mathbf{x}, \quad \mathbf{A}^{\mathbf{F}}_{ij} = \int_{\tilde{\Omega}} \nabla N_i^{\tilde{\Omega}}(\mathbf{x}) \cdot \nabla N_j^{\tilde{\Omega}}(\mathbf{x}) d\mathbf{x}, \quad i, j \in \mathfrak{S},$$

where \mathfrak{S} denotes the set of the total number of degrees of freedom (DOF) in $\tilde{\Omega}$. The set \mathfrak{S} can be naturally split as $\mathfrak{S} = \mathfrak{S}_I \cup \mathfrak{S}_{\mathcal{B}}$, where \mathfrak{S}_I is the set of the internal DOF and $\mathfrak{S}_{\mathcal{B}}$ is the set of the mesh nodes lying on the artificial boundary \mathcal{B} , respectively.

The (rectangular) matrices

$$\mathbf{Q}_{ij} = \int_{\mathcal{B}} \gamma_{\mathcal{B}} N_i^{\tilde{\Omega}}(\mathbf{x}) N_j^{\mathcal{B}}(\mathbf{x}) d\mathbf{x}, \quad i \in \mathfrak{S}, \quad j \in \mathfrak{S}_{\mathcal{B}}$$

and

$$\mathbf{B}(t)_{ij} = \int_{\Gamma(t)} \gamma_{\Gamma(t)} N_i^{\tilde{\Omega}}(\mathbf{x}) N_j^{\Gamma(t)}(\mathbf{x}) d\mathbf{x}, \quad i \in \mathfrak{S}, \quad j \in \mathfrak{S}_{\Gamma}$$

represent the discrete trace operators defined on \mathcal{B} and $\Gamma(t)$, respectively. We remark that, for simplicity, the computation of the matrices \mathbf{M}^F , \mathbf{A}^F , \mathbf{Q} and \mathbf{B} has been performed by approximating the domain $\tilde{\Omega}$ and the curves $\Gamma(t)$ and \mathcal{B} with the polygon $\tilde{\Omega}_\Delta$ and the polygonal functions $\Gamma_\Delta(t)$ and \mathcal{B}_Δ , associated to the corresponding approximation meshes defined on $\tilde{\Omega}$, $\Gamma(t)$ and \mathcal{B} , respectively. In this case, the approximation error should also take into account the approximation of the geometry (see [12]).

For the time discretization of (30), we consider a uniform partition of the interval $[0, T]$ into N subintervals; we denote by $t_n, n = 0, \dots, N$ the time instants, by Δ_t the temporal step size of the decomposition and by $\mathbf{B}^n = \mathbf{B}(t_n)$. Introducing the new variable $\mathbf{v} = \dot{\mathbf{u}}$, we apply the Crank-Nicolson integration method to the first equation of (30), thus obtaining

$$\begin{cases} \mathbf{M}^F \left(\frac{\mathbf{v}^{n+1} - \mathbf{v}^n}{\Delta_t} \right) + \mathbf{A}^F \left(\frac{\mathbf{u}^{n+1} + \mathbf{u}^n}{2} \right) - \left(\frac{\mathbf{B}^{n+1} \boldsymbol{\lambda}_\Gamma^{n+1} + \mathbf{B}^n \boldsymbol{\lambda}_\Gamma^n}{2} \right) - \mathbf{Q} \left(\frac{\boldsymbol{\lambda}_\mathcal{B}^{n+1} + \boldsymbol{\lambda}_\mathcal{B}^n}{2} \right) = \frac{\mathbf{f}^{n+1} + \mathbf{f}^n}{2} \\ \frac{\mathbf{v}^{n+1} + \mathbf{v}^n}{2} = \frac{\mathbf{u}^{n+1} - \mathbf{u}^n}{\Delta_t} \\ (\mathbf{B}^{n+1})^T \mathbf{u} = \mathbf{0}. \end{cases}$$

From the above second relation we get $\mathbf{v}^{n+1} = \frac{2}{\Delta_t}(\mathbf{u}^{n+1} - \mathbf{u}^n) - \mathbf{v}^n$ which, inserted in the first relation, leads to

$$\begin{cases} \left(\mathbf{M}^F + \frac{\Delta_t^2}{4} \mathbf{A}^F \right) \mathbf{u}^{n+1} - \frac{\Delta_t^2}{4} \mathbf{B}^{n+1} \boldsymbol{\lambda}_\Gamma^{n+1} - \frac{\Delta_t^2}{4} \mathbf{Q} \boldsymbol{\lambda}_\mathcal{B}^{n+1} = \left(\mathbf{M}^F - \frac{\Delta_t^2}{4} \mathbf{A}^F \right) \mathbf{u}^n \\ \quad + \frac{\Delta_t^2}{4} \mathbf{B}^n \boldsymbol{\lambda}_\Gamma^n + \frac{\Delta_t^2}{4} \mathbf{Q} \boldsymbol{\lambda}_\mathcal{B}^n + \Delta_t \mathbf{M}^F \mathbf{v}^n + \frac{\Delta_t^2}{4} (\mathbf{f}^{n+1} + \mathbf{f}^n) \\ (\mathbf{B}^{n+1})^T \mathbf{u}^{n+1} = \mathbf{0} \\ \mathbf{v}^{n+1} = \frac{2}{\Delta_t}(\mathbf{u}^{n+1} - \mathbf{u}^n) - \mathbf{v}^n. \end{cases} \quad (31)$$

By properly reordering the unknown elements of \mathbf{u}^n , we can write the unknown vector $\mathbf{u}^n = [\mathbf{u}_I^n, \mathbf{u}_\mathcal{B}^n]^T$, whose two components \mathbf{u}_I^n and $\mathbf{u}_\mathcal{B}^n$ represent the unknowns associated with the internal nodes and with those on the boundary \mathcal{B} , respectively. Similarly it can be done for the vector \mathbf{v}^n and for the matrices \mathbf{M}^F , \mathbf{A}^F , \mathbf{Q} and \mathbf{B}^n . These latter can be rewritten in the following block forms:

$$\mathbf{M}^F = \begin{bmatrix} \mathbf{M}^F_{II} & \mathbf{M}^F_{IB} \\ \mathbf{M}^F_{BI} & \mathbf{M}^F_{BB} \end{bmatrix}, \quad \mathbf{A}^F = \begin{bmatrix} \mathbf{A}^F_{II} & \mathbf{A}^F_{IB} \\ \mathbf{A}^F_{BI} & \mathbf{A}^F_{BB} \end{bmatrix}, \quad \mathbf{Q} = \begin{bmatrix} \mathbf{Q}_{IB} \\ \mathbf{Q}_{BB} \end{bmatrix}, \quad \mathbf{B}^n = \begin{bmatrix} \mathbf{B}_{I\Gamma}^n \\ \mathbf{B}_{B\Gamma}^n \end{bmatrix}.$$

Equation (31) is finally coupled with the discretized NRBC equation (29) (or with (??) if the collocation method is used for the spatial discretization of the NRBC). To summarize, the final scheme reads:

starting from the initial values \mathbf{u}^0 , \mathbf{v}^0 , $\boldsymbol{\lambda}_\Gamma^0$ and $\boldsymbol{\lambda}_\mathcal{B}^0$, compute the unknowns $\mathbf{u}^{n+1} =$

$[\mathbf{u}_I^{n+1}, \mathbf{u}_B^{n+1}]^T, \mathbf{v}^{n+1} = [\mathbf{v}_I^{n+1}, \mathbf{v}_B^{n+1}]^T, \boldsymbol{\lambda}_\Gamma^{n+1}$ and $\boldsymbol{\lambda}_B^{n+1}$ such that

$$\begin{cases} \left(\mathbf{M}^F + \frac{\Delta_t^2}{4} \mathbf{A}^F \right) \mathbf{u}^{n+1} - \frac{\Delta_t^2}{4} \mathbf{B}^{n+1} \boldsymbol{\lambda}_\Gamma^{n+1} - \frac{\Delta_t^2}{4} \mathbf{Q} \boldsymbol{\lambda}_B^{n+1} = \left(\mathbf{M}^F - \frac{\Delta_t^2}{4} \mathbf{A}^F \right) \mathbf{u}^n \\ \quad + \frac{\Delta_t^2}{4} \mathbf{B}^n \boldsymbol{\lambda}_\Gamma^n + \frac{\Delta_t^2}{4} \mathbf{Q} \boldsymbol{\lambda}_B^n + \Delta_t \mathbf{M}^F \mathbf{v}^n + \frac{\Delta_t^2}{4} (\mathbf{f}^{n+1} + \mathbf{f}^n) \\ (\mathbf{B}^{n+1})^T \mathbf{u}^{n+1} = 0 \\ \mathbf{v}^{n+1} = \frac{2}{\Delta_t} (\mathbf{u}^{n+1} - \mathbf{u}^n) - \mathbf{v}^n \\ 2\mathbf{V}_0 \boldsymbol{\lambda}_B^{n+1} - (\mathbf{M}^B + 2\mathbf{K}_0) \mathbf{u}_B^{n+1} = 2 \sum_{j=0}^n \mathbf{K}_{n-j} \mathbf{u}_B^j - 2 \sum_{j=0}^n \mathbf{V}_{n-j} \boldsymbol{\lambda}_B^j. \end{cases}$$

for $n = 0, \dots, N-1$.

Remark 3.1. The boundary matrix \mathbf{B}^n depends on the time instant t_n since the boundary Γ_n changes its position at each time step. From the computational point of view, this implies that at each time step t_n the intersections between the triangular (fixed) mesh of $\tilde{\Omega}$ with the boundary segments of $\Gamma(t_n)$ have to be recomputed. To this aim, we refer the reader to the recent papers [10] and [26], where the authors present algorithmic details concerning the intersection of triangular and boundary grids. This computational overhead is however negligible, if compared to a global re-meshing of the bidimensional domain in a standard finite element approach. Finally, we remark that condition (17) guarantees that the rank of the matrix \mathbf{B}^n is maximum.

Remark 3.2. Since the boundary $\Gamma(t_n)$ represents the contour of a physical obstacle, it is natural, from the computational point of view, to set equal to zero the numerical solution u^n (which is computed in the whole enlarged domain) at those grid points that at the time step t_n are internal to the boundary $\Gamma(t_n)$. Such a procedure may cause, in principle, strong discontinuities of the solution in those points that at time t_n are covered by the obstacle, while at time t_{n+1} are no more internal to it.

This drawback is avoided by considering a rotation velocity of the obstacle smaller than that of the wave propagation, as it is natural to assume in many realistic situations. To give an idea, we consider three examples in which the scatterers consist of blades rotating in air or in water. It is known that the velocity of propagation of acoustic waves in air and in water is $c \approx 343 \text{ m/sec}$ and $c \approx 1500 \text{ m/sec}$, respectively. The periferic velocity v_p of a rotor, whose blades have radius R , is given by $v_p = 2\pi \cdot n_r \cdot R$, where n_r is the number of revolutions of the rotor.

i) The periferic velocity v_p of the rotor blades of an helicopter, with $R = 4 \text{ m}$ and $n_r = 600$ revolutions per minute (rpm) (10 revolutions per second), is $v_p = 2\pi \cdot 10 \cdot 4 \text{ m/sec} \approx 251 \text{ m/sec}$, while a signal in air propagates, approximately, at 343 m/sec .

ii) An eolic aerogenerator, with $R = 45 \text{ m}$, and performing $n_r = 15$ rpm, has a periferic velocity $v_p = 2\pi \cdot 15/60 \cdot 45 \text{ m/sec} \approx 71 \text{ m/sec}$.

iii) An aircraft rotor, with $R = 0.5 \text{ m}$, and performing $n_r = 5700$ rpm has a periferic velocity $v_p = 2\pi \cdot 5700/60 \cdot 0.5 \text{ m/sec} \approx 300 \text{ m/sec}$, while a signal in water propagates, approximately, at 1500 m/sec .

We further note that, in case i), the ratio $v_p/c \approx 0.73$ (see Example 4).

4 Numerical results

In this section we present five numerical tests. In the first example we consider the Poisson problem and we study the convergence in space of the FEM-BEM fictitious domain approach in a case where the exact solution is known. This test is performed to validate the analysis carried out in Section 2 where, we recall, the weak formulation in space of the NRBC is considered. For completeness, we compare the results with those obtained when the strong formulation of the NRBC is considered, and a collocation method is used instead of the Galerkin one for the spatial approximation. We remark that the latter formulation is certainly more appealing from the computational point of view, since its numerical approximation makes it highly competitive with existing NRBCs of local type.

In the Examples 2–5 we consider the time dependent wave equation. In particular, in Example 2, we consider a fix scatterer and, to test the accuracy of the approximation obtained by the fictitious domain approach, we construct a reference “exact” solution by applying the standard Lubich-collocation boundary element method described in [19] with a very fine space and time discretizations. Once the density function is retrieved on the physical obstacle, the solution at any point in the infinite domain is computed by means of the associated potential (see [19] for details). This solution will be denoted by the acronym BEM. In Examples 3 and 4 we apply the proposed scheme to the diffraction of a wave by single or multiple rotating bodies. In the last Example 5, we consider two rotating bodies and a wave that impinges upon them, and is generated by two sources that are located out of the finite computational domain. The test is performed to simulate those situations where one is interested in knowing the solution at points that are far away from sources; in this case, the NRBC that we propose allows to choose a computational domain that does not include the sources, and easily allows to treat such external contributions.

Example 1. Let Γ and \mathcal{B} be the circles centered at the origin and having radius 2 and 10, respectively. Let Ω be the domain bounded internally by Γ and externally by \mathcal{B} . We denote by $u(\mathbf{x}) = u(x, y) = e^{-5((x-5)^2+y^2)}$ the exact solution of the Laplace equation

$$\begin{cases} -\Delta u(x, y) &= f(x, y) & \text{in } \Omega \\ u(x, y) &= g(x, y) & \text{on } \Gamma, \end{cases}$$

where the source $f(x, y) = -e^{-5((x-5)^2+y^2)}(100(x-5)^2 + 100y^2 - 20)$ and $g = u|_{\Gamma}$. We remark that, in principle, the source f does not have a compact support and $g \neq 0$, which contradicts our assumptions. However, since f decays exponentially fast away from its center $x = (5, 0)$, it can be regarded as compactly supported from the computational point of view, and g can be treated as zero along Γ . Moreover, the compatibility conditions of the data along Γ are satisfied, and the solution u is regular in the whole enlarged domain.

We consider the enlarged domain $\tilde{\Omega}$ represented by the disk bounded by \mathcal{B} . We discretize it by a uniform triangulation, and we denote by $h^{\tilde{\Omega}}$ its mesh size and by $n_{T, \tilde{\Omega}}$ the number of triangles of the decomposition. Starting from the initial mesh corresponding to the choice $h_{\tilde{\Omega}} \approx 0.3$, the successive triangulations are obtained by halving the mesh size $h_{\tilde{\Omega}}$ (which implies that the number of triangles $n_{T, \tilde{\Omega}}$ is multiplied by a factor 4 at each refinement).

We denote by $u_{h_{\tilde{\Omega}}}^{\text{Fict}}$ the approximate solution obtained by applying the fictitious FEM-BEM coupling method, using the Galerkin approach for the approximation in space of the NRBC. Being the exact solution known, we compute the relative H^1 error defined by

$$\text{Err}_{H^1}^{\text{Fict}} = \frac{\|u - u_{h_{\tilde{\Omega}}}^{\text{Fict}}\|_{H^1(\tilde{\Omega})}}{\|u\|_{H^1(\tilde{\Omega})}}.$$

We also compute the relative L^2 error defined by

$$\text{Err}_{L^2}^{\text{Fict}} = \frac{\|u - u_{h_{\tilde{\Omega}}}^{\text{Fict}}\|_{L^2(\tilde{\Omega})}}{\|u\|_{L^2(\tilde{\Omega})}}.$$

In Table 1 we report the relative errors and the associated expected orders of convergence (EOC) corresponding to the decomposition of the boundary Γ into $M_\Gamma = 32$ segments.

Table 1: Example 1. Relative H^1 and L^2 errors for the Galerkin method associated to the fictitious FEM-BEM method and corresponding EOC.

$h_{\tilde{\Omega}}$	$n_{T,\tilde{\Omega}}$	$\text{Err}_{H^1}^{\text{Fict}}$	$\text{EOC}_{H^1}^{\text{Fict}}$	$\text{Err}_{L^2}^{\text{Fict}}$	$\text{EOC}_{L^2}^{\text{Fict}}$
3.06E-01	4272	4.58E-01	0.98	1.95E-01	1.92
1.53E-01	17088	2.32E-01		5.18E-02	
7.65E-02	68352	1.17E-01	0.99	1.33E-02	1.96
3.82E-02	273408	5.87E-02	1.00	3.35E-03	1.99

We have applied the fictitious FEM-BEM coupling method also using the collocation approach for the approximation in space of the NRBC, and the errors we have obtained are very similar to those obtained in Table 1.

For completeness, we compare the above errors with the ones obtained by applying the standard FEM-BEM coupling method, where the problem is solved in the effective computational domain Ω , and the Dirichlet boundary condition on Γ is enforced strongly. We denote by

$$\text{Err}_{H^1}^{\text{Strong}} = \frac{\|u - u_{h_\Omega}^{\text{Strong}}\|_{H^1(\Omega)}}{\|u\|_{H^1(\Omega)}} \quad \text{and} \quad \text{Err}_{L^2}^{\text{Strong}} = \frac{\|u - u_{h_\Omega}^{\text{Strong}}\|_{L^2(\Omega)}}{\|u\|_{L^2(\Omega)}},$$

where $u_{h_\Omega}^{\text{Strong}}$ denotes the corresponding approximate solution obtained by applying the Galerkin method for the spatial approximation of the NRBC. These errors are shown in Table 2. We remark that the effective computational domain Ω is different from the enlarged one $\tilde{\Omega}$ of the fictitious domain approach. Consequently, the triangular meshes are different, as well as the corresponding number of triangles $n_{T,\Omega}$ and $n_{T,\tilde{\Omega}}$ and of the mesh sizes h_Ω and $h_{\tilde{\Omega}}$. Therefore, we compare the errors obtained by the two approaches for comparable values of the mesh refinement parameters $h_{\tilde{\Omega}}$ and h_Ω . As it can be seen, the fictitious domain method and the strong formulation provide the same accuracy for comparable values of the mesh size.

Table 2: Example 1. Relative errors for the Galerkin method associated to the FEM-BEM method where the Dirichlet conditions on Γ are enforced strongly, and the corresponding EOC.

h_Ω	$n_{T,\Omega}$	$\text{Err}_{H^1}^{\text{Strong}}$	$\text{EOC}_{H^1}^{\text{Strong}}$	$\text{Err}_{L^2}^{\text{Strong}}$	$\text{EOC}_{L^2}^{\text{Strong}}$
3.04E-01	4166	4.69E-01	0.95 0.99 1.00	2.92E-01	1.97
1.52E-01	16664	2.40E-01		7.47E-02	2.03
7.59E-02	66656	1.21E-01		1.83E-02	2.01
3.80E-02	266624	6.06E-02		4.60E-03	

Example 2. In this second test we solve Problem (18) in a case of a fix obstacle, represented by a disk of radius 2. In this case the boundary Γ (the circumference of radius 2) and \mathcal{O}^e do not depend on t . The wave propagates radially, starting from an initial configuration $u_0(x, y) = e^{-5((x-5)^2+y^2)}$, with null initial velocity and without external source ($v_0 = 0$, $f = 0$). Even if the exact solution in this case is not known, this is a good test to validate the fictitious FEM-BEM coupling method, since the numerical solution can be compared to the solution obtained by using well known and reliable methods. In particular we use here the reference solution obtained by applying the BEM. For the comparison with other methods, see [16].

Although u_0 does not have a local support, it decays exponentially fast away from its center $x = (5, 0)$, in such a way that, from the computational point of view, it can be regarded as compact and supported in a disk with radius smaller than 3 (at distance 2.7 from its center it assumes approximately values of the order $1.0\text{E-}16$). We choose the artificial boundary \mathcal{B} as a circle of radius $R = 10$, so that $\tilde{\Omega}$ is the domain bounded internally by Γ and externally by \mathcal{B} , and the enlarged domain $\tilde{\tilde{\Omega}}$ is the disk bounded by \mathcal{B} . In Figure 4 we show the snapshots of the solution obtained by using the fictitious domain approach at some time instants. In Figure 5, left plot, we show the good agreement of the solution obtained by the fictitious approach with the reference one (BEM) at $P \approx (10, 0) \in \mathcal{B}$ and for $t \in [0, 20]$. The approximate solution has been obtained by a decomposition of the domain $\tilde{\Omega}$ into 68724 triangles and by choosing a uniform partition of Γ into 128 segments. With such a choice the spatial step sizes are $h \approx 7.6e - 02$ and $\delta \approx 9.8e - 02$. Here and in the following numerical tests, we have noticed that the factor β of Lemma 2.7 is approximately 1. The time interval has been decomposed into $N = 256$ time steps. We note that the solution, represented in Figure 5, is zero until the initial data reaches the artificial boundary (around $t = 4$). Approximately at time $t = 2.5$, the wave reaches the boundary Γ and is reflected back, so that around $t = 9$ we see another outgoing wave at the artificial boundary \mathcal{B} . After that time, the wave is completely out of the annulus, as the reference solution and the approximate solution with the exact NRBC show. In the right plot we show the energy of the system. Since the system is a conservative one, the energy remains constant for the time

instants $t \in [0, 4]$ after which it dissipates because the wave reaches the artificial boundary and leaves the finite computational domain. It is worthwhile noting that the wave hits the obstacle approximatively at $t = 2.5$ but, since the obstacle is fix, the energy is perfectly preserved up to $t \approx 4$.

Figure 4: Example 2: Snapshots of the solution at different times.

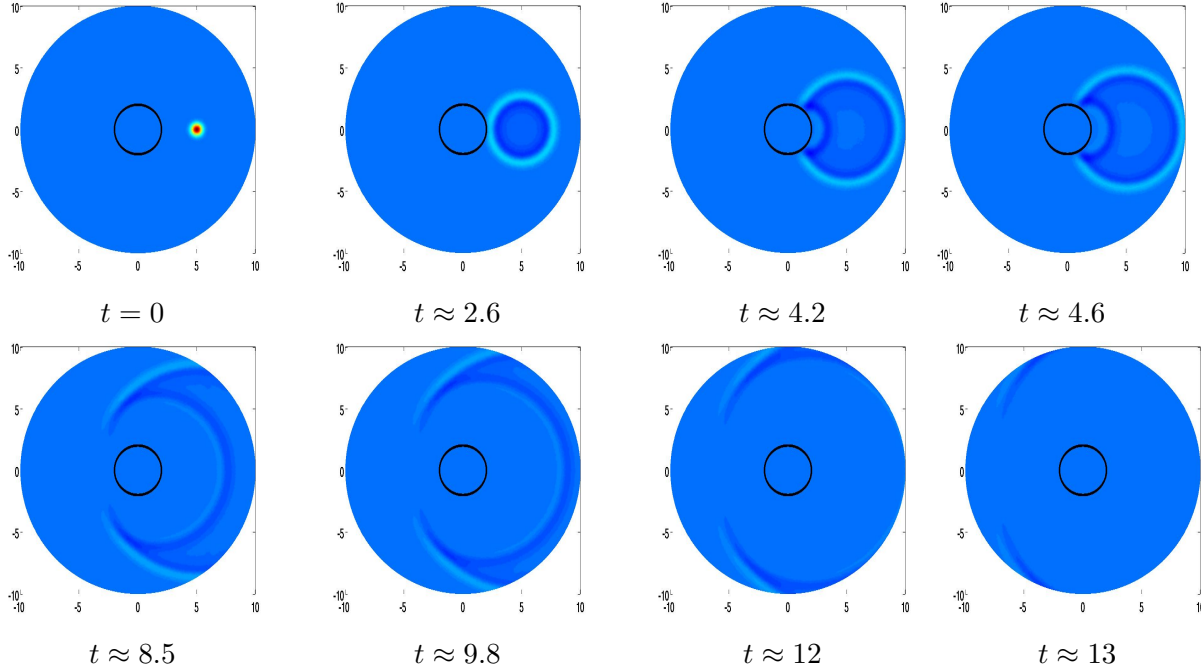
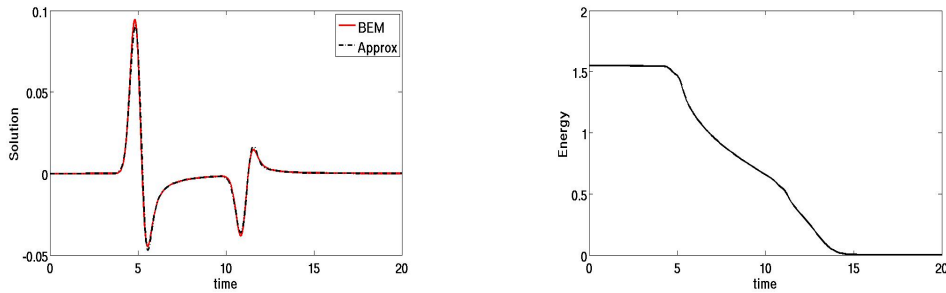


Figure 5: Example 2. Behavior of the solution at $P \approx (10, 0)$ (left plot) and energy dissipation (right plot).



In the next three examples we apply the proposed scheme to the diffraction of a wave by rotating bodies, so that the state of the obstacles depends on t . We recall that boundary element methods seem difficult to apply to such types of problem and standard finite elements would require the reconstruction of the computational mesh at each time step. To avoid such complexity, the fictitious domain approach seems a very attractive solution. In this case in fact, the computational overhead, with respect to the case of a fix obstacle, is simply given

by the computation of the boundary matrix \mathbf{B}^n , which has to be recomputed at each time step because the boundary Γ changes its position.

Example 3. We consider a soft ellipsoidal obstacle whose boundary $\Gamma_0 = \Gamma(t = 0)$ is the ellipse given by the parametric representation

$$\begin{cases} x_0 = 2 \cos(\theta) \\ y_0 = \sin(\theta). \end{cases} \quad \theta \in [0, 2\pi)$$

The scatterer rotates anticlockwise around its center, with a constant angular velocity equals to $\omega = 2\pi/20$. Therefore $\Gamma(t)$ has the following parametric representation:

$$\begin{bmatrix} x(t) \\ y(t) \end{bmatrix} = \begin{bmatrix} \cos(\omega t) & -\sin(\omega t) \\ \sin(\omega t) & \cos(\omega t) \end{bmatrix} \begin{bmatrix} x_0 \\ y_0 \end{bmatrix}$$

with $t \in [0, T]$. We consider a wave with the initial configuration u_0 as in Example 2 and that impinges upon the rotating obstacle with null initial velocity. The transparent artificial boundary \mathcal{B} is the circle of radius 10. In Figure 6 we show the snapshots of the solution at different time instants. In Figure 8 we show the behavior of the solution at a point $P \approx (10, 0)$ that belongs to the artificial boundary \mathcal{B} (left plot) and the energy behavior of the system with respect to time (right plot). The space/time discretization parameters are the same of Example 2. The wave hits the rotating obstacle around $t = 3.5$, and the energy is preserved up to the time instant $t \approx 5$, when the wave reaches the transparent boundary and leaves the computational domain. We remark that, even if in this case the system is not a conservative one, the velocity of rotation of the obstacle is small if compared to the speed of propagation of the wave, so that the energy remains constant until the wave leaves the computational domain.

We have proposed the fictitious FEM-BEM coupling method in the case of a single obstacle and when the non vanishing data are included in the finite computational domain. In the following two examples we show that the proposed approach can be easily extended to the case of multiple obstacles and multiple sources, where the latter are not included in the finite computational domain, rather they are treated by the NRBC.

Example 4. We consider two scatterers, both having helicoidal shape, that rotate around their own center with constant angular velocity $\omega = 2\pi/20$ and in opposite directions (clockwise direction for the left obstacle and anticlockwise direction for the right one). The initial configuration of the two obstacles is given by the parametric representations

$$\begin{cases} x_0 = c_i + \rho(\theta) \cos(\theta - \pi/2) \\ y_0 = \rho(\theta) \sin(\theta - \pi/2), \end{cases} \quad \theta \in [0, 2\pi]$$

where

$$\rho(\theta) = \frac{1}{3} \frac{1}{\sqrt{\left| \cos\left(\frac{3}{4}\theta\right) \right|^{13} + \left| \sin\left(\frac{3}{4}\theta\right) \right|^{13}}},$$

Figure 6: Example 3: Snapshots of the solution at different times.

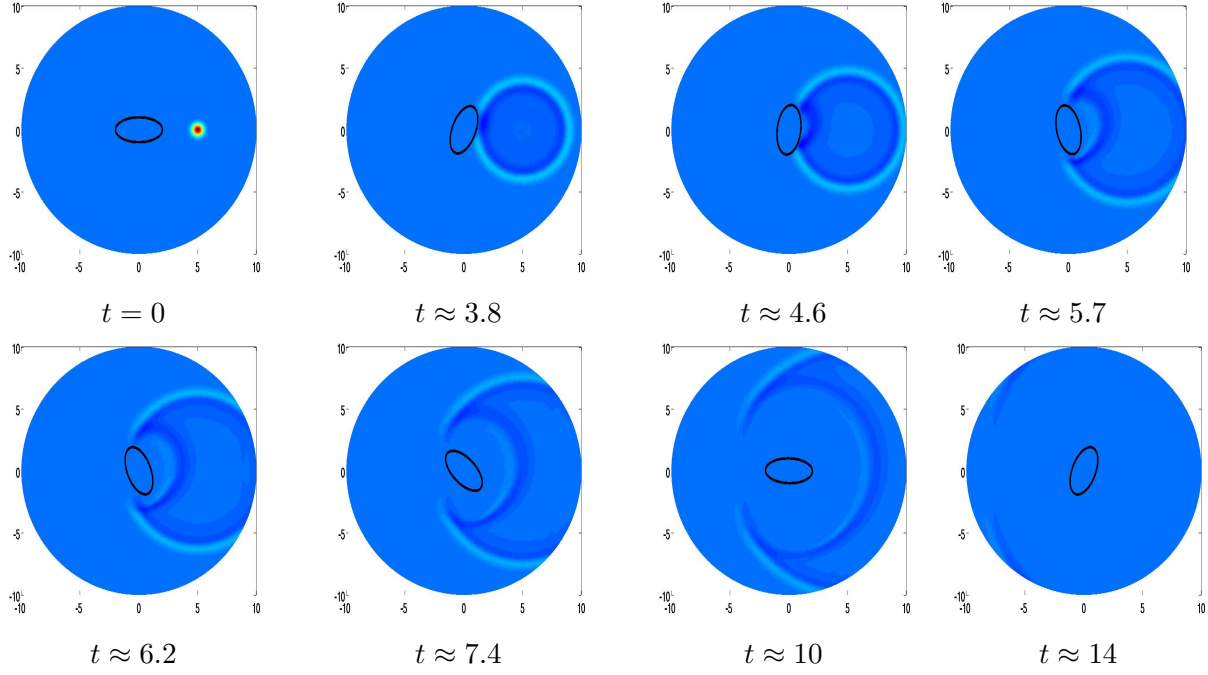
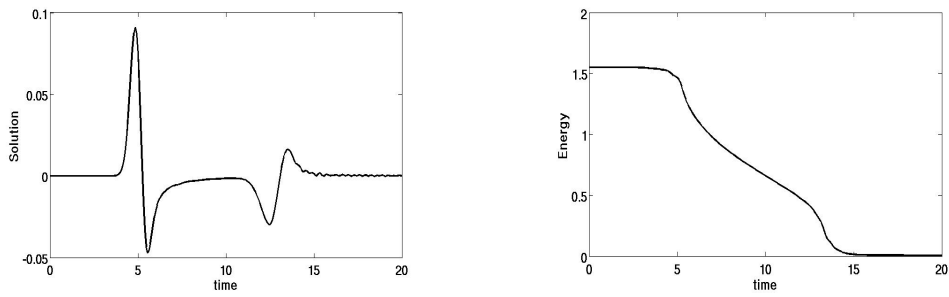


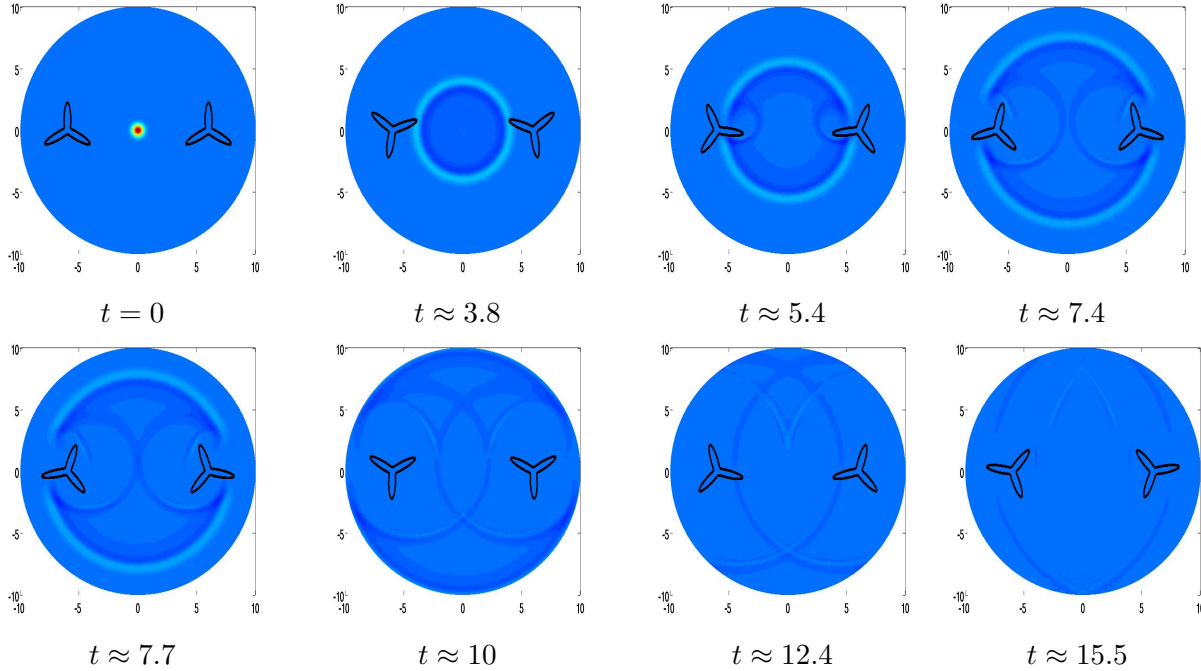
Figure 7: Example 3. Behavior of the solution at $P \approx (10, 0)$ (left plot) and energy dissipation (right plot).



$c_1 = 6$ and $c_2 = -6$ for the right and the left obstacles, respectively. We note that the length of the blades of the scatterers is $R \approx 2.24$ ($= \rho(\pi)$), and that the number of revolutions per second is $n_r = 1/20$. Therefore, the periferic velocity $v_p = 2\pi n_r R \approx 0.71 \text{ m/sec}$. Since the velocity of the (scaled in time) problem is $c = 1$, the ratio $v_p/c \approx 0.71$ (see Remark 3.2, i)).

The two obstacles are surrounded by an artificial circular boundary of radius 10. The initial configuration of the wave is given by the function u_0 of Examples 2 and 3, now centered at the origin of the axis. In Figure 8 we show the snapshots of the propagation of the wave at some instants. In Figure 9, left plot, we show the behavior of the solution at a point $P \approx (0, 4)$ for $t \in [0, 20]$ and in the right plot the energy of the system. The solution has been obtained by a decomposition of $\tilde{\Omega}$ into 69176 triangles, by choosing a uniform partition of the two boundaries of the obstacles into 60 segments and with $N = 256$ time steps. In this case, since the system is not a conservative one, we observe that the energy increases after the wave hits the two obstacles (around $t = 4$) and is reflected back.

Figure 8: Example 4. Snapshots of the solution at different times.

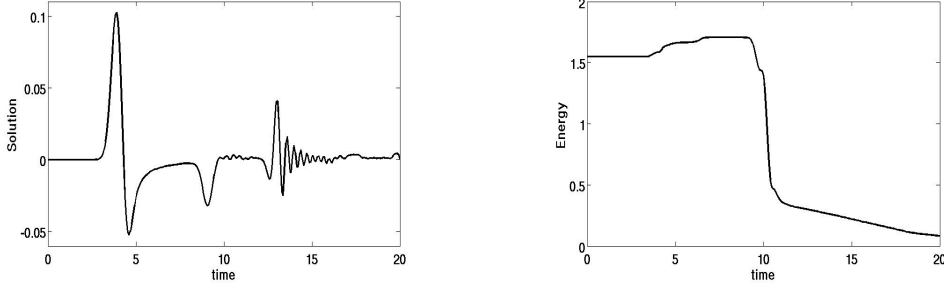


Example 5. To conclude our numerical tests, we consider the two helicoidal scatterers of Example 4, rotating with constant angular velocity $\omega = 2\pi/40$. We solve Problem (18) with initial null configuration and initial null velocity. The wave is generated by two sources $f_1(\mathbf{x}, t) = h(t)\delta(\mathbf{x} - \mathbf{x}_1)$ and $f_2(\mathbf{x}, t) = h(t)\delta(\mathbf{x} - \mathbf{x}_2)$, where

$$h(t) = e^{-t} \sin(100t).$$

The two sources are concentrated at the points $\mathbf{x}_1 = (0, 12)$ and $\mathbf{x}_2 = (0, -24)$. We choose, as artificial boundary, the circumference of radius 10. Therefore, the two sources are located

Figure 9: Example 4. Behavior of the solution at $P \approx (0, 4)$ (left plot) and energy dissipation (right plot).



out of the finite computational domain, and the corresponding contribution to the wave propagation is taken into account in the NRBC, which assumes the following form

$$\frac{1}{2}u(\mathbf{x}, t) - \mathbf{V}\lambda_{\mathcal{B}}(\mathbf{x}, t) + \mathbf{K}u(\mathbf{x}, t) = I_f(\mathbf{x}, t) \quad \text{in } \mathcal{B} \times (0, T].$$

Because of the presence of the Dirac function in f_1 and f_2 , the integration in space in the volume term (see [17])

$$I_f(\mathbf{x}, t) = \int_0^t \int_{\text{supp}(f)} f(\mathbf{y}, \tau) G(\mathbf{x} - \mathbf{y}, t - \tau) d\mathbf{y} d\tau, \quad (32)$$

disappears and I_f has the following simple form:

$$I_f(\mathbf{x}, t) = I_{f_1}(\mathbf{x}, t) + I_{f_2}(\mathbf{x}, t) = \int_0^t h(\tau) G(\mathbf{x} - \mathbf{x}_1, t - \tau) d\tau + \int_0^t h(\tau) G(\mathbf{x} - \mathbf{x}_2, t - \tau) d\tau.$$

For the computation of the volume integral I_f , we apply the Lubich convolution technique. We recall that, if the sources are much more far from the area of interest, the approach that consists in choosing an artificial boundary sufficiently large to include them, thus wasting computational time and space memory. In Figure 10 we show the snapshots of the wave propagation at some instants. In Figure 11, left and middle plot, we show the behavior of the solution at the points $P \approx (0, 4)$ and $P \approx (0, -4)$ for $t \in [0, 80]$, respectively, and in the right plot the energy of the system. The solution has been obtained by a decomposition of $\tilde{\Omega}$ into 69176 triangles, by choosing a uniform partition of the two boundaries of the obstacles into 64 segments and with $N = 512$ time steps. We note that the energy of the system is null until $t \approx 2.5$, that is when the wave produced by the source f_1 enters the computational domain. Then the energy starts increasing and is also influenced by the wave generated by the source f_2 , whose contribution appears around $t \approx 13$, after which the waves produced by the two sources start overlapping and mixing to the waves reflected back by the scatterers. Then, the energy decreases and vanishes because the two sources have an exponential decay to zero. Therefore, after $t \approx 60$ the waves are completely out of the computational domain and the system is at rest.

Figure 10: Example 5. Snapshots of the solution at different times.

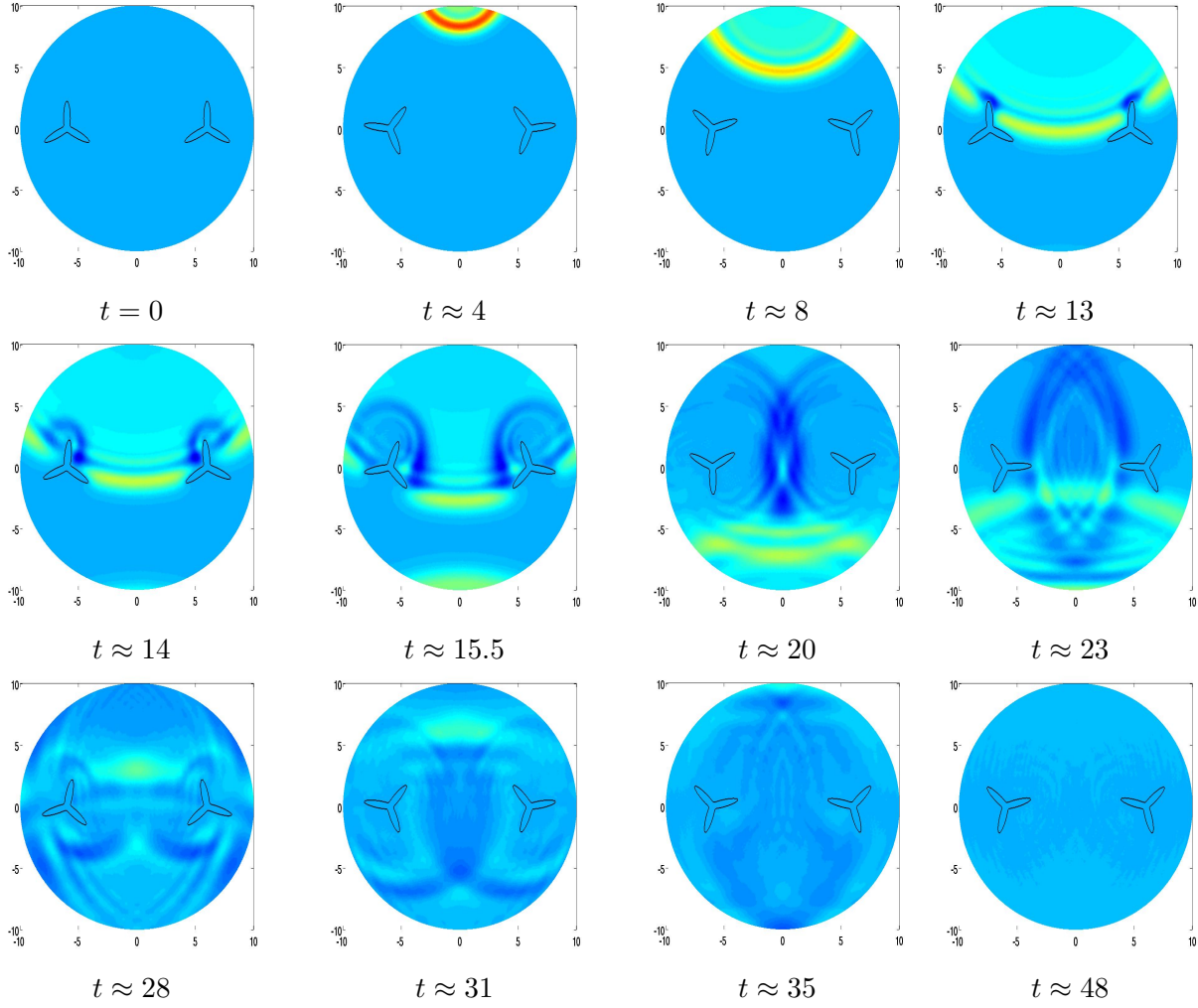
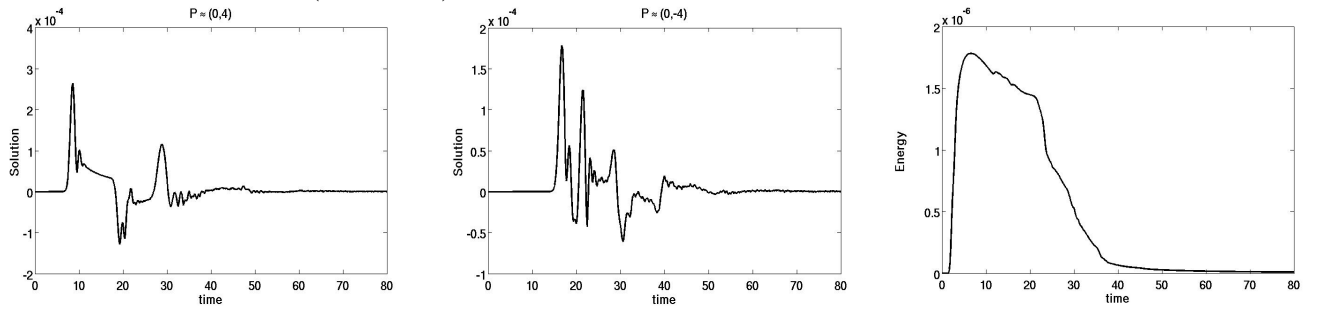


Figure 11: Example 5. Behavior of the solution at $P \approx (0, 4)$ (left plot), $P \approx (0, -4)$ (middle plot) and energy dissipation (right plot).



5 Conclusions

We have considered a fictitious domain method for the solution of wave propagation problems in unbounded domains, treating also the presence of rotating rigid obstacles, coupled with a NRBC on a suitably chosen artificial boundary. For its solution, we have used a standard finite element method coupled with an unconditionally stable time marching scheme for the approximation of the domain method, and a Galerkin (collocation) method in space in space coupled with a convolution quadrature technique in time for the approximation of the NRBC. We have presented the analysis and convergence results for the Poisson problem. The coupling of the two schemes is new and, although fictitious domain methods have been successfully applied to time dependent problems with stationary obstacles, there is no much work on numerical methods for the treatment of moving scatterers. At the moment the theory to justify the validity of the presented approach in the full space-time formulation is still at an early stage, but the numerical results we have obtained are very promising. We have presented the application of such an approach to a wide range of problems, treating also multiple rotating obstacles and multiple sources that are located far away from the computational domain of interest.

Acknowledgements

The author gratefully acknowledges the two referees for their careful reading of the manuscript and their useful remarks.

References

- [1] T. Abboud, P. Joly, J. Rodríguez, and I. Terrasse. Coupling discontinuous Galerkin methods and retarded potentials for transient wave propagation on unbounded domains. *J. Comput. Phys.*, 230(15):5877–5907, 2011.
- [2] C. Atamian, Q.V. Dinh, R. Glowinski, J. He, and J. Périaux. Control approach to fictitious-domain methods application to fluid dynamics and electromagnetics. In *Fourth International Symposium on Domain Decomposition Methods for Partial Differential Equations*, SIAM, Philadelphia, pages 275–309, 1991.
- [3] I. Babuška. The finite element method with Lagrange multipliers. *Numer. Math.*, (20):179–192, 1973.
- [4] L. Banjai, A. R. Laliena, and F.J. Sayas. Fully discrete Kirchhoff formulas with CQ-BEM. *IMA J. Numer. Anal.*, 35(2):859–884, 2015.
- [5] L. Banjai, C. Lubich, and F.J. Sayas. Stable numerical coupling of exterior and interior problems for the wave equation. *Numer. Math.*, 129(4):611–646, 2015.
- [6] Y. Bazilevs and T.J.R. Hughes. Nurbs-based isogeometric analysis for the computation of flows about rotating components. *Comput. Mech.*, 43:143–150, 2008.

- [7] E. Bécache, P. Joly, and C. Tsogka. Fictitious domains, mixed finite elements and perfectly matched layers for 2-D elastic wave propagation. *J. Comput. Acoust.*, 9(3):1175–1201, 2001.
- [8] S. Bertoluzza, M. Ismail, and B. Maury. Analysis of the fully discrete fat boundary method. *Numer. Math.*, 118(1):49–77, 2011.
- [9] F. Brezzi and M. Fortin. *Mixed and Hybrid Finite Element Methods*. Springer Series in Computational Mathematics. Springer-Verlag, 1991.
- [10] E. Burman, S. Claus, P. Hansbo, M. G. Larson, and A. Massing. CutFEM: Discretizing geometry and partial differential equations. *Int. J. Numer. Meth. Engng*, 104(7):472–501, 2015.
- [11] P. G. Ciarlet. *The finite element method for elliptic problems*. North-Holland, Amsterdam, 1978.
- [12] P. G. Ciarlet. *Finite Element Methods (Part 1)*, volume 2 of *Handbook of Numerical Analysis*, pages 23–351. North-Holland, 1991.
- [13] F. Collino, P. Joly, and F. Millot. Fictitious domain method for unsteady problems: application to electromagnetic scattering. *J. Comput. Phys.*, 138(2):907–938, 1997.
- [14] W. Dahmen and A. Kunoth. Appending boundary conditions by Lagrange multipliers: analysis of the LBB condition. *Numer. Math.*, 88(1):9–42, 2001.
- [15] G. Dziuk and C. M. Elliott. Finite element methods for surface PDEs. *Acta Numer*, 22:289–396, 2013.
- [16] S. Falletta and G. Monegato. An exact non reflecting boundary condition for 2D time-dependent wave equation problems. *Wave Motion*, 51(1):168–192, 2014.
- [17] S. Falletta and G. Monegato. Exact nonreflecting boundary conditions for exterior wave equation problems. *Publ. Inst. Math.*, 96:103–123, 2014.
- [18] S. Falletta and G. Monegato. Exact non-reflecting boundary condition for 3D time-dependent multiple scattering-multiple sources problems. *Wave Motion*, 58:281–302, 2015.
- [19] S. Falletta, G. Monegato, and L. Scuderi. A space-time BIE method for nonhomogeneous exterior wave equation problems. The Dirichlet case. *IMA J. Numer. Anal.*, 32(1):202–226, 2012.
- [20] S. Falletta, G. Monegato, and L. Scuderi. A space-time BIE method for wave equation problems: the (two-dimensional) Neumann case. *IMA J. Numer. Anal.*, 34(1):390–434, 2014.
- [21] V. Girault and R. Glowinski. Error analysis of a fictitious domain method applied to a Dirichlet problem. *Japan J. Indust. Appl. Math*, 12:487–524, 1995.

- [22] D. Givoli. *Numerical Methods for Problems in Infinite Domains*. Elsevier, Amsterdam, 1992.
- [23] D. Givoli. Recent advances in the dtn fe method. *Archives of Computational Methods in Engineering*, 6:71–116, 1999.
- [24] D. Givoli. High-order local non-reflecting boundary conditions: A review. *Wave Motion*, 39:319–326, 2004.
- [25] R. Glowinski, T.W. Pan, and J. Périaux. A fictitious domain method for Dirichlet problem and applications. *Comput. Methods Appl. Mech. Engrg.*, 111(3-4):283–303, 1994.
- [26] J. Grande and A. Reusken. A higher order finite element method for partial differential equations on surfaces. *SIAM J. Numer. Anal.*, 54(1):388–414, 2016.
- [27] M.J. Grote and Ch. Kirsch. Nonreflecting boundary condition for time-dependent multiple scattering. *J. Comput. Phys.*, 221:41–62, 2007.
- [28] M.J. Grote and I. Sim. Local nonreflecting boundary condition for time-dependent multiple scattering. *J. Comput. Phys.*, 230:3135–3154, 2011.
- [29] C. Johnson and J.C. Nédélec. On the coupling of boundary integral and finite element methods. *Math. Comp.*, 35(152):1063–1079, 1980.
- [30] Ch. Lubich. Convolution quadrature and discretized operational calculus. I. *Num. Math.*, 52:129–145, 1988.
- [31] Ch. Lubich. On the multistep time discretization of linear initial-boundary value problems and their boundary integral equations. *Num. Math.*, 67:365–389, 1994.
- [32] Ch. Lubich and D. Mansour. Variational discretization of wave equations on evolving surfaces. *Math. Comp.*, 84(292), 2015.
- [33] M.S. Mommer. A smoothness preserving fictitious domain method for elliptic boundary-value problems. *IMA J. Numer. Anal.*, 26(3), 2006.
- [34] A. Nitsche. Ein kriterium für die quasi-optimalität des ritzschen verfahren. *Num. Math.*, 11:346–348, 1968.
- [35] S. A. Sauter and C. Schwab. *Boundary element methods*. Springer-Verlag, Berlin, 2011.
- [36] P. Silvester and M. S. Hsieh. Finite-element solution of 2-dimensional exterior-field problems. In *Proc. Inst. Electr. Engrs*, pages 1743–1746, 1971.
- [37] A. Taflové and S.C. Hagness. *Computational Electrodynamics. The finite-difference time-domain method*. Boston-London, 2005.
- [38] Y. Zhang. A fictitious domain method for acoustic wave propagation problems. *Mathematical and Computer Modelling*, 50:351–359, 2009.

- [39] W. P. Ziemer. *Weakly Differentiable Functions*. Springer-Verlag, 1989.
- [40] O. C. Zienkiewicz, D. W. Kelly, and P. Bettess. The coupling of the finite element method and boundary solution procedures. *Internat. J. Numer. Methods Engrg*, 11:355–375, 1977.